A multiwavelength erbium-ytterbium co-doped fiber laser

By
Mansour Dastmalchi

A thesis submitted to the faculty of graduate studies
Lakehead University
in partial fulfillment of the requirements for the degree of
Masters of Science in Physics

Department of Physics
Lakehead University
August 2007

Your file Votre référence
ISBN: 978-0-494-31824-9
Our file Notre référence
ISBN: 978-0-494-31824-9

Abstract

A fiber ring laser, using erbium-ytterbium co-doped double clad fiber is proposed and demonstrated to produce a medium power multiwavelength fiber laser. The experimental results show that the ring resonator configuration can produce more output power compared to a laser based on bidirectional pumping scheme in Fabry-Perot resonator configuration. To stabilize the lasing lines we used an unpumped erbium doped fiber as saturable absorber. A sagnac loop interferometer is used as a filter inside the cavity and its effect has been explored. We can produce a maximum four lasing lines which are stable for more than 2 hours when observed through OSA with a resolution of 0.05 nm. The maximum output power obtained from the laser is more than 100 mW. Our best result at room temperature is simultaneous oscillations of two single-mode laser wavelengths with a maximum output power of 60 mW when observed through a scanning Fabry-Perot spectrum analyzer of resolution 27 MHz.

Acknowledgement

I take this opportunity to express my gratitude to my beloved parent and my wife for their moral support during my study in Lakehead University. I am deeply indebted to my supervisor Dr. G. Das, for his constant support. Without his help and advice this work would not be possible. I would like to thank Dr. S.N. Sarkar, Jean-Marc Lachaine, Jonas Valiunas, Zachari Medendorp for their advice and help. I would also like to thank all faculty members in Physics department who enriched my knowledge through my whole study in this department.

Content

List of Graphs

List of Tables

Chapter 1

1.1 Introduction

With the invention of "Laser", the idea of communicating by light became more attractive than ever. Since the use of laser for free space optical communication proved limited due to scattering, absorption, etc., tremendous efforts were made to find a light wave carrier. After the fabrication of glass fiber in 1966 by Kao and Hockham [1], the proposals for optical communication via dielectric waveguide became more promising.

In practice, dielectric waveguides used for optical communications are highly flexible fibers made of Silicon Dioxide known as Silica(SiO_2). Today a number of dopants or impurities are used to modify the refractive index of Silica. They help researchers to achieve desired spectral characteristics.

1.1.1 Structure of an optical fiber

Figure 1.1(a) shows an optical fiber which consists of a cylindrical core cladded

by a material of slightly lower refractive index and surrounded by a protective jacket. The ray propagates following total internal reflection.

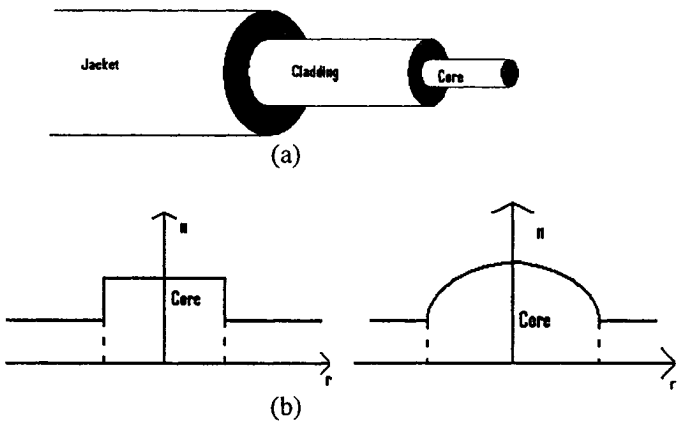

Figure 1.1 (a) An Optical Fiber (b) Step and Graded refractive index Profile

The core refractive-index "n" (figure 1.1(b)) can be uniform or graded, while the cladding index is typically uniform.

1.1.2 Characteristics of fibers

The fundamental characteristics of an optical fiber such as interaction of light with active ions in doped fiber [2], splice loss, micro-bending loss, dispersion etc. while traveling through fiber, can be determined from the modal field distribution. In order to analyze the modal behavior in a circularly symmetric cross section fiber, we consider a step index fiber with uniform cylindrical dielectric core of radius "ρ" and step-refractive index profile of

$$\begin{aligned} n(\mathrm{r}) &= n_{co} && 0 \le r < \rho \\ n(\mathrm{r}) &= n_{cl} && \rho < r < \infty \end{aligned} \qquad (1.1)$$

The general wave equation derived from Maxwell's equations reduced to a scalar wave equation under weakly guiding approximation ($n_{co} \approx n_{cl}$) [3]. The scalar wave equation satisfied by the electric and magnetic fields is given by

$$\nabla^2 \psi = \varepsilon_0 \mu_0 n^2 \left(\frac{\partial^2 \psi}{\partial t^2} \right) \tag{1.2}$$

where ψ stands for both electric and magnetic fields. The solution of the above equation for electric field can be obtained in cylindrical coordinates as

$$\vec{E}(r,\varphi,z,t) = \vec{e_t}(r,\varphi) \exp i(\omega t - \beta z)$$

$$\vec{e_t}(r,\varphi) = e_x(r,\varphi)\hat{x} + e_y(r,\varphi)\hat{y} \tag{1.3}$$

Using separation of variable method, the equation (1.2) is reduced to [4]

$$\frac{r^2}{R}\left(\frac{d^2R}{dr^2} + \frac{1}{r}\frac{dR}{dr} \right) + r^2\left[n^2(r)k_0 - \beta^2 \right] = -\frac{1}{\phi}\frac{d^2\phi}{d\varphi} = l^2 \tag{1.4}$$

The ϕ - dependence is of the form of $Cos\, l\varphi$ or $Sin\, l\varphi$ for l =0,1,2,3,....

and the complete field is given by,

$$\begin{pmatrix} e_x(r,\varphi) \\ e_y(r,\varphi) \end{pmatrix} = R(r) \exp i(\omega t - \beta z) \begin{Bmatrix} Cos\, l\varphi \\ Sin\, l\varphi \end{Bmatrix} \tag{1.5}$$

The above radial part "R(r)" would be solutions of the following equations ,

$$r^2 \frac{d^2R}{dr^2} + r\frac{dR}{dr} + \left(U^2 \frac{r^2}{\rho^2} - l^2 \right) R = 0 \qquad r < \rho$$

$$r^2 \frac{d^2R}{dr^2} + r\frac{dR}{dr} - \left(W^2 \frac{r^2}{\rho^2} + l^2 \right) R = 0 \qquad r > \rho \tag{1.6}$$

where U and W as well as normalized frequency V are,

$$U = \rho\left(k_0^{\,2} n_{co}^{\,2} - \beta^2\right)^{\frac{1}{2}}$$

$$W = \rho\left(\beta^2 - k_0^{\,2} n_{cl}^{\,2}\right)^{\frac{1}{2}} \qquad (1.7)$$

$$V = \left(\mathrm{U}^2 + W^2\right)^{\frac{1}{2}} = k_0\, \rho\left(n_{co}^{\,2} - n_{cl}^{\,2}\right)^{\frac{1}{2}}$$

For wave guidance, propagation constant β in equation (1.7) must be within the range of $k_0 n_{cl} \le \beta \le k_0 n_{co}$. Under this condition, the radial part of field in equation (1.6) can be expressed by Bessel functions inside the core and modified Bessel functions in the cladding, as given below,

$$\begin{pmatrix} e_x(r,\varphi) \\ e_y(r,\varphi) \end{pmatrix} = \begin{cases} \dfrac{A}{J_\nu(U)} J_\nu\left(\dfrac{Ur}{\rho}\right) \begin{Bmatrix} Cos\, l\varphi \\ Sin\, l\varphi \end{Bmatrix} & r < \rho \\ \dfrac{A}{K_\nu(W)} K_\nu\left(\dfrac{Wr}{\rho}\right) \begin{Bmatrix} Cos\, l\varphi \\ Sin\, l\varphi \end{Bmatrix} & r > \rho \end{cases} \qquad (1.8)$$

So we can have two independent plane polarized wave as e_x or e_y, and also considering its azimutal dependency of $Cos\, l\varphi$ and $Sin\, l\varphi$ we can have four degenerate modes for $l > 0$ and two degenerate modes for $l = 0$ which are orthogonal with respect to each other. Here degeneracy means that separate field functions exist for same β. The modes are known as "linearly polarized" modes because under weakly guiding approximation, the longitudinal component of electric and magnetic fields are very small compared to

transverse component. Continuity condition of the field and its derivative at the core cladding interface leads to the following eigenvalue equations given by,

$$U\frac{J_{l+1}(U)}{J_l(U)} = W\frac{K_{l+1}(W)}{K_l(W)}$$

Or (1.9)

$$U\frac{J_{l-1}(U)}{J_l(U)} = -W\frac{K_{l-1}(W)}{K_l(W)}$$

For every l, we have m number of β and the Linearly Polarized modes designated as LP_{lm}.

In exact analysis of the vector wave equation [5], the longitudinal component of electric and magnetic fields are finite and they produce **HE(** $|h_z|$ **>>**$|e_z|$**>0), EH(** $|e_z|$ **>>**$|h_z|$**>0) , TE$_{0m}$ (e_z=0)** and **TM$_{0m}$(h_z=0)** modes. The Figure 1.2 shows numerical solution of exact modal analysis [5].

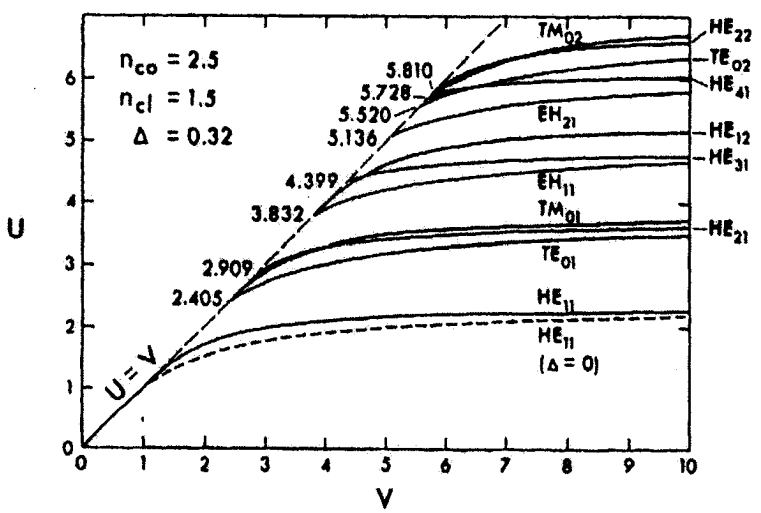

Figure 1.2 Numerical solution of the eigenvlue equations for first twelve modes.

The values along the dashed line are the cutoff values [5].

Further, the Figure 1.3 shows analysis based on weakly guiding approximation [5].

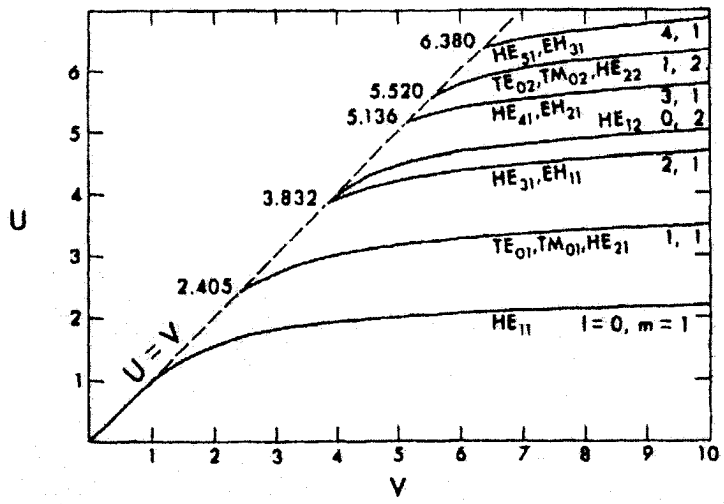

Figure 1.3 Numerical solution of the eigenvalue equations for first twelve modes considering Weakly Guiding Approximation[5]

Comparing the Figures 1.2 and 1.3, we can conclude that any LP_{lm} modes is a combination of vector modes ($HE_{l+1,m}$ and $EH_{l-1,m}$) with identical β. So if we group them according to their degeneracies they will correspond to each other like;

$$\begin{gathered} HE_{11} \rightarrow LP_{01} \\ HE_{21};TM_{01};TE_{01} \rightarrow LP_{11} \\ HE_{12} \rightarrow LP_{02} \\ HE_{22};TM_{02};TE_{02} \rightarrow LP_{12} \\ HE_{13} \rightarrow LP_{03} \\ HE_{23};TM_{03};TE_{03} \rightarrow LP_{13} \\ HE_{14} \rightarrow LP_{04} \end{gathered} \tag{1.10}$$

The condition $W \rightarrow 0$ in equation (1.9) corresponds to cut-off of the guided modes. For $l = 0$ equation (1.9) reduces to $J_1(V_c) = 0$ which gives cut off values of all

LP_{0m} modes. Similarly from equation (1.9) $J_0(V_c) = 0$ corresponds to LP_{1m} modes. For LP_{11} V_c is 2.405 which is the first root of $J_0(V_c)$. However, first root of $J_1(V_c)$ is zero. So for $0<V_c<2.405$ (Figure 1.4) the fiber will support only the LP_{01} mode.

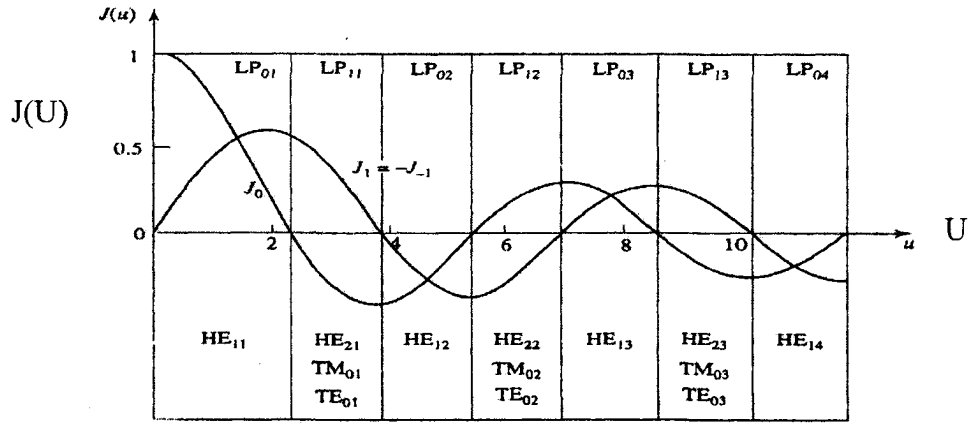

Figure 1.4 The allowed cut off values of different modes [6]

1.2 Mode field diameter (MFD)

Mode field diameter is the parameter used to evaluate transmission characteristics of optical fiber like splice loss [7] and is a measure of the spot size or beam width of light propagating in a single mode fiber. It is a function of wavelength, core radius and refractive index profile which can be used to predict the fraction of power propagating in the core. For step-index and graded-index single mode fibers, considering "$\bar{\omega}$" as the mode field radius of light, we can define MFD as

$$MFD = 2\bar{\omega} = 2\left[\frac{\int_0^\infty r^2\psi^2(r)dr}{\int_0^\infty r\,\psi^2(r)\,dr}\right]^{\frac{1}{2}} \tag{1.11}$$

The fundamental modal field distribution is very important to predict several important parameters used in communication. To overcome the complexity of numerical calculations, Gaussian function is introduced to replace the exact field as given below

$$\psi(r) = \psi_0 \exp\left(\frac{-r^2}{\bar{\omega}^2}\right) \tag{1.12}$$

where $\psi(r)$ corresponds to modal field distribution (equation 1.8) for fundamental mode. For a step index fiber, $0.8 \leq V \leq 2.5$, we can find $\bar{\omega}$ by using empirical expression below [8]

$$\bar{\omega} = \rho\left[0.65 + \frac{1.619}{V^{\frac{3}{2}}} + \frac{2.879}{V^6}\right] \tag{1.13}$$

1.3 Dispersion

As the pulse propagates through an optical fiber, it gets broadened. This spreading comes from two factors one is known as intermodal dispersion due to propagation delay of various modes in multimode fiber and the other one intramodal dispersion which exists as "Material Dispersion" and "Waveguide Dispersion".

Different modes have different propagation constants which leads to time lag or in another word different rays have different incident angle into fiber so rays travel a particular length of fiber at different times. However such intermodal dispersion in multimode fibers may be reduced by using an optimum refractive index

profile. A graded or parabolic refractive index profile gives a tremendous bandwidth advantage over multimode step index fibers. Different modes travel at different velocity. The envelope of these signals which propagates at group velocity is given by [9]

$$V_g = \frac{d\beta}{dk}$$

where β is propagation constant and k is wave number in free space. The group index of material for a plane wave carrier in a dispersive medium with the refractive index "n" is given by

$$N \equiv \frac{d\beta}{dk} = \frac{d(kn)}{dk} \tag{1.14}$$

Now we consider a fiber with a core index n_1 and the cladding index n_2, and using previous definitions for U, W, V, we define b the normalized propagation constant as

$$b = 1 - \frac{U^2}{V^2}$$

Using these equations ,

$$\beta = k\left(n_2^{\,2} + \left(n_1^{\,2} - n_2^{\,2}\right)b\right)^{\frac{1}{2}} \tag{1.15}$$

Differentiating with respect to $k(n_1, n_2, b)$ and considering

$$n >> k\frac{dn}{dk} \qquad \Rightarrow N_1 \cong n_1 \;\&\; N_2 \cong n_2 \tag{1.16}$$

we get

$$\frac{d\beta}{dk} = N_2 + \left(N_1 - N_2\right)\left(\frac{d(Vb)}{dV}\right) \tag{1.17}$$

The corresponding pulse spread can be obtained from the derivative of group velocity with respect to"k" and considering approximation in equation (1.16), we get

$$\frac{d^2\beta}{dk^2} = \frac{dN_2}{dk} + \frac{V}{k}(N_1 - N_2)\frac{d^2(Vb)}{dV^2} \tag{1.18}$$

First part of the above equation characterizes "the material dispersion" which is same for all modes and the second part $\frac{d^2(Vb)}{dV^2}$ represents the group delay that would be different for different modes. For small values of V, $\frac{d(Vb)}{dV}$ is very small and for large values of V it approaches unity, basically the higher the mode number, the higher the time lag $\left(\left(\frac{d(bV)}{dV}\right)\right)$. In other word, the higher the mode number the slower the energy transport [6] .In conclusion, for $V < 1$ the transmitted pulse would be distorted and change its form and duration, therefore we have like a propagation of uniform plane wave in an infinitely extended medium whose refractive index equals that of fiber cladding. In another word, for small V most of power is transmitted in cladding. However, for large V the second term in equation (1.18) becomes considerable and changes the power distribution between core and cladding in such a way that most of the power would flow in core.

For an arbitrary refractive index profile, the equation (1.18) will contain one more term which corresponds to "Profile Dispersion" taking care of profile shape's radial variation. If the refractive index profile is

$$n(x,y) = n_1[1 - 2\Delta f(x,y)]^{\frac{1}{2}}$$
$$\Delta = \frac{n_1^2 - n_2^2}{2n_1^2}, \tag{1.19}$$

Considering profile dispersion parameter , $\frac{d\Delta}{dk}$, which shows variation of refractive index profile with wavelength and n_1 and n_2 which are the maximum index of core and cladding, the expression for dispersion reduces to [10] ,

$$D_p = N_2 \frac{d\Delta}{dk}\left[V\frac{d^2(bV)}{dV^2} + \frac{d(bV)}{dV} - b\right] \tag{1.20}$$

1.4 Polarization-maintaining fibers

The state of electro magnetic vibration inside the fiber which is commonly denoted by polarization is not preserved inside circular core fibers. In some applications preserving polarization of light is required.

The most common way to make polarization-preserving fibers which can hold or maintain the optical wave amplitude in a particular polarization state to a relatively high degree along the entire length is to use birefringent materials. Birefringence is introduced in a fiber whenever the circular symmetry of the ideal fiber is broken by creating an anisotropic refractive index distribution in the core region. This asymmetry can result from either a geometrical deformation of the core or a material anisotropy through various elasto-optic, magneto-optic or electro-optic index change. In non-circular core fibers, the light travels fastest when polarized along the direction of minimum polarizability. The smallest transverse dimension of the core is the fast axis of the birefringence. For specific core shape, birefringence as well as two non-degenerate orthogonal polarization eigenmodes (along fast and slow axises) can be calculated [11].

The principal axes X,Y are determined by the symmetry elements of the cross section. The larger the anisotropy of the cross section, the greater the difference in propagation constants β_x and β_y for two normal modes; so the birefringence B for an optical wavelength of λ is given by

$$B = \frac{(\beta_x - \beta_y)\lambda}{2\pi} \tag{1.21}$$

So the phase retardation along "z" is

$$\varphi = (\beta_x - \beta_y)z \tag{1.22}$$

When this phase difference is an integer number of 2π the two modes will beat and at this point the input polarization state will be reproduced.

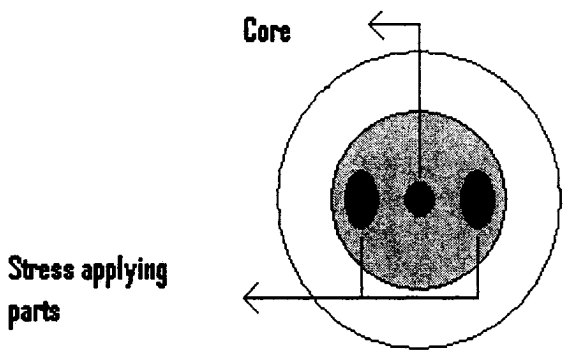

Figure 1.5 Panda Fiber

The length over which this beating occurs is the fiber beat length defined as,

$$L = \frac{2\pi}{\beta} \tag{1.23}$$

One of the high-birefringent fibers which is fabricated using lateral stress is PANDA fiber which is widely used because it has a low transmission loss and good polarization maintaining characteristics. The stress applying portion is produced from a material having a relatively large coefficient of thermal expansion. Therefore when the polarization maintaining optical fiber is produced by melting and drawing, the core is

subjected to different degrees of stress from transverse and longitudinal directions during glassification as a result of which large distortions are anisotropicaly generated in the core which causes birefringence in the polarization maintaining fiber [12,13].

1.5 Doped fibers

In general a gain medium is required to amplify a signal. Based on desired wavelengths and applications of such wavelengths, experts use different bulk active media. In optical fibers we dope the core by rare earth elements and use them as gain medium in fiber amplifiers and lasers. The absorption and emission cross sections of dopant ions in the Silica fiber depend on polarization states[14,15]. The polarization property of a fiber laser is characterized by the degree of polarization (DOP) defined as [16]

$$DOP = \frac{I_{max} - I_{min}}{I_{max} + I_{min}} \tag{1.24}$$

I_{max} and I_{min} are related to maximum and minimum polarization intensities and clearly $0 \leq DOP \leq 1$. Based on some characteristics such as high gain and wide bandwidth region with applications [17] in communication network, material processing, etc., system users and designers are using different rare-earth doped fibers. Among all rare-earth family members, only a few elements satisfy important criteria for laser applications like having the laser transition wavelength at the region of 1.0 or 1.5 μm which corresponds to optical fiber communications. Based on such criteria Er^{+3} ; Yb^{+3} ; $Er^{+3} - Yb^{+3}$ are widely used.

The rare earth ions are considered in two groups of "Lanthanides" and "Actinides" of which only Lanthanide elements are used as dopants in optical fibers. In a glass matrix, the rare earth elements form trivalent ions with electron structure of ;

$$1s^2 2s^2 2p^6 3s^2 3p^6 3d^{10} 4s^2 4p^6 4d^{10} 4f^N 5s^2 5p^6 \qquad N = 1,..., 14$$

$$N \ for \quad Er^{+3} = 11$$

$$N \ for \quad Yb^{+3} = 13$$

all visible and infrared transition come from the "4f" layer. In order to show the energy level of these ions we use the notation of $^{2S+1}L_J$ in which

L ≡ angular momentum; S,P,D,F,G,H,I,K,,.... stand for L=0,1,2,3,4,5,6,7,....

S ≡ total spin

J ≡ total angular momentum

Figure1.6 shows energy level diagram for Er^{+3} in which $^4I_{\frac{15}{2}} \rightarrow {}^4I_{\frac{11}{2}}$ (pumped at 980 nm)

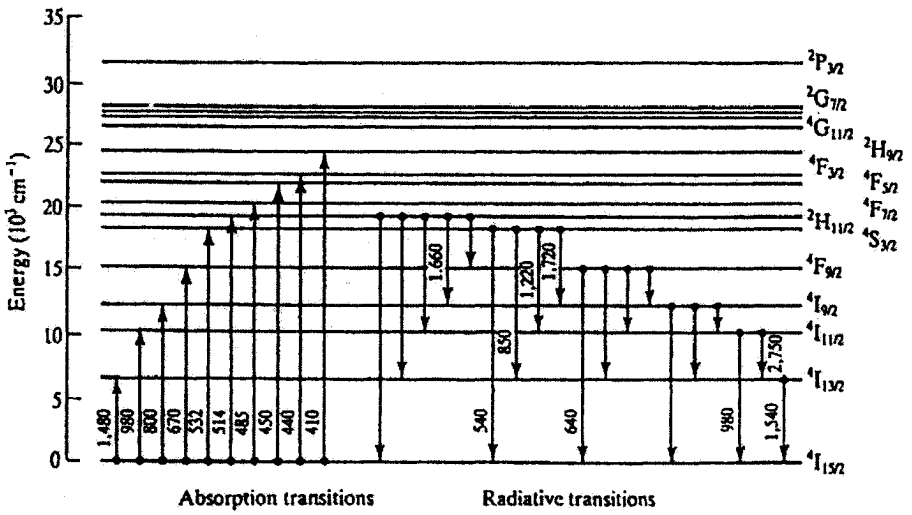

Figure 1.6 Energy level diagram of Er:glass with absorption and radiative transitions[18]

is the pump transition and $^4I_{\frac{13}{2}} \rightarrow {}^4I_{\frac{15}{2}}$ is the stimulated emission transition as a three-

level laser. But Erbium-doped fiber laser operating in the spectral region of 1550 nm can be optically pumped at 800, 980 and 1480 nm or visible wavelengths such as 532 nm.

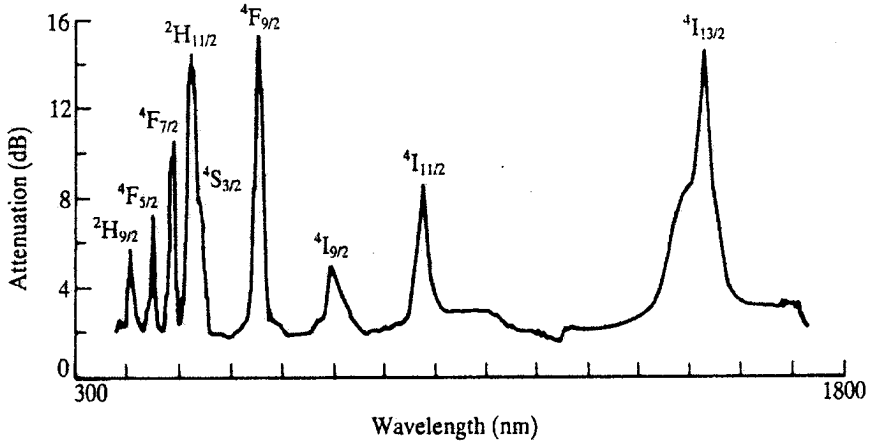

Figure 1.7 Typical absorption spectrum of aluminosilicate Er-doped fiber[18]

The spectroscopy of Er ions in glass hosts has a crucial role in understanding the gain spectrum and power conversion efficiency. So the spectroscopic study of Er: glass gives us understanding about radiative and non - radiative atomic decay, laser line broadening and exited state absorption.

1.5.1 Laser line broadening

The spectral line width of an optical transition of rare-earth ions in SiO_2 is broadened due to two effects

- Life time broadening

Each level in atom is labeled by a particular life time which can be described by corresponding spectral line width $(\Delta\omega)$. The life time broadened laser lines resulting from all atomic contribution is said to be homogeneous; in another word, all ions (atoms)in medium host experience the same broadening effects.

- Stark splitting

The other cause of broadening is Stark splitting which is induced by the Crystalline Electric Field surrounding the rare earth ion and can remove the degeneracy of levels

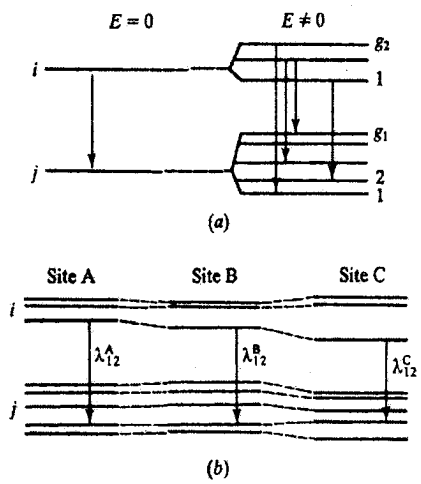

Figure 1.8 (a) Effect of Stark splitting of energy levels with degeneracies g_1 and g_2 caused by crystalline electric field E (b)effect of inhomogeneous broadening [18]

Since in a glass host the field randomly varies from site-to-site the stark splitting between energy levels is also random. The site-to-site variation causes inhomogeneous line broadening. As mentioned earlier, based on quantum mechanical rules, the degeneracy of states is g= 2J+1 but based on Kramers' Rule in the presence of electric field, the maximum number of Stark sublevels is $g = J + \frac{1}{2}$. According to this rule, the Stark levels for ${}^4I_{\frac{15}{2}}$ and ${}^4I_{\frac{13}{2}}$ in Er^{+3} are g_1=8 and g_2=7 respectively. But the actual number of sublevels depends on the symmetry of the Crystalline Electric Field. In the case of purely random host structure corresponding to no symmetry, we expect to observe the maximum number of Stark components given by Kramers' Rule. Because of Stark

splitting; there is $g_1 * g_2$ possible transitions between the stark sublevels which leads us to have a wide gain spectrum .

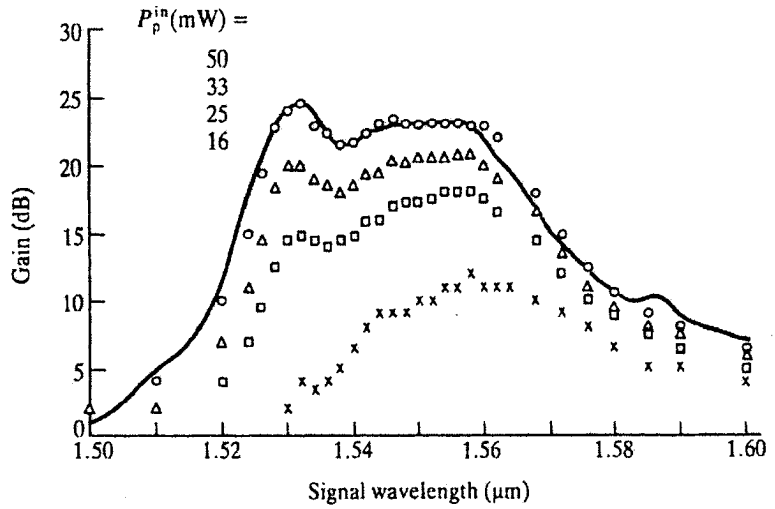

Figure 1.9 Gain spectrum profile of Er:glass fiber[18]

1.6 Overlap integral

The efficiency of an optical fiber amplifier depends on the efficient interaction of spatial mode distribution of a pump or a signal with the distribution of dopant ions. The highest overlap of pump and dopant distribution would happen if firstly, the pump modes have small spatial mode size and secondly we concentrate the dopants into the centre portion of the optical modes where the intensity is the highest. Considering these conditions, the overlap integral is defined as [2],

$$\Gamma_k = \int_0^{2\pi} d\varphi \int_0^b I_k(r,\varphi) r\, dr \tag{1.25}$$

In which $I_k(r, \varphi)$ is normalized

modal intensity which is proportional to square of mode field distribution. The radius of the doped region can be expressed as,

$$b_{eff} = \left[\frac{1}{2} \int_0^{2\pi} d\varphi \int_0^{\infty} \frac{n_t(r)}{n_t(0)} r \, dr \right]^{\frac{1}{2}} \tag{1.26}$$

where $n_t(r)$ is dopant distribution function in core. The population density for each energy level is[18],

$$\overline{n_i(z)} = \frac{\int_0^{2\pi} \int_0^{\infty} n_i(r, \phi, Z) \, r \, dr \, d\varphi}{\pi b_{eff}^2}, \quad i = 1,2 \tag{1.27}$$

The overlap integral is given by

$$\Gamma_{k,i} = \frac{\int_0^{2\pi} \int_0^{\infty} I_k(r,\varphi) \, n_i(r,\varphi,z) \, r \, dr \, d\varphi}{\overline{n_i(z)}} \qquad i = 1,2 \tag{1.28}$$

Considering Gaussian function for fundamental mode and uniform doped region of radius "b" equation (1.28) is reduced to[2]

$$\Gamma_{K,1} = \frac{-Ln\left(\frac{P_k \exp\left(\frac{-b^2}{w^2} \right) + 1}{P_k + 1} \right)}{P_k \left(1 + \frac{w^2}{b^2} \, Ln\left(\frac{P_k \exp\left(\frac{-b^2}{w^2} \right) + 1}{P_k + 1} \right) \right)} \tag{1.29}$$

where p_k is normalized optical power and Figure1.10 shows the variation of $\Gamma_{K,1}$

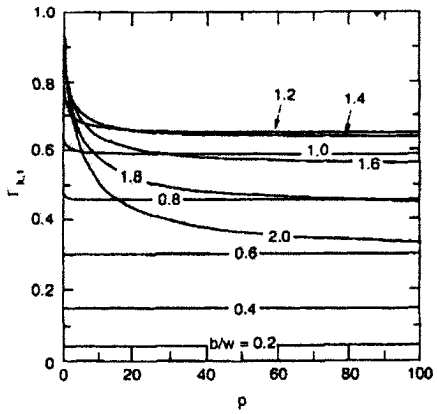

Figure 1.10 Power-dependent ($P = P_k$) over lap integral $\Gamma_{k,1}$ for a Gaussian mode approximation [2]

Vs. P. So we can conclude that if $b < w$, Γ would be constant and less than 0.6 .

1.7 Fiber lasers

By employing a piece of doped fiber in a resonator and having it pumped by a laser, we can produce lasing wavelengths in the visible or infrared region of electromagnetic spectrum. The fiber lasers have some advantages compared to bulk optics systems like compact size, high efficiency and high beam quality. The lasers in time-domain can categorize into two groups "Continuous Wave Fiber Lasers" or "Pulsed Fiber Lasers", and in wavelength domain as single wavelength(SW) or multi wavelength(MW).

1.7.1 Single wavelength fiber laser

A single wavelength source has attracted great attention regarding some application like coherent communication and spectroscopy. Fiber lasers in a simple

standing wave geometry can not usually generate a single frequency output due to spatial hole-burning effect. Because of this effect, different standing –wave patterns in a Fabry-Perot resonator saturate different parts of gain medium individually (along "z"). So two adjacent axial modes would be able to oscillate simultaneously. Furthermore, there is inhomogeneous broadening in rare-earth doped fiber. It arises from variations in center frequency and line width of ions in physically different sites at which different longitudinal modes at different frequencies can burn hole in gain spectrum separately which is called "Spectral Hole Burning". The first single longitudinal mode was achieved in one effort that the cavity length was shortened so that multimode operation due to spatial and spectral hole burning was eliminated [19]. In some reports a monomode single lasing line was constructed using two intracore Bragg reflector for cavity to discriminate longitudinal modes causing spectral hole burning[20,21,22].We can even enhance the situation by using a short standing wave cavity combined with one or two narrow-band Bragg grating that select a single longitudinal mode[23]. Several methods have been proposed using a unidirectional ring cavity[24,25] to produce single wavelength fiber laser.

1.7.2 Multiwavelength fiber laser

Optical fiber networks employing wavelength-division multiplexing (WDM) are promising for optical fiber communication systems. For such systems and for other purposes like sensing or high resolution spectroscopy, many wavelengths oscillating simultaneously are highly desirable. As mentioned earlier rare-earth doped laser materials, possessing split Stark sublevels with multiple allowed transitions provide the

possibility of having oscillations at more than one wavelength. The reason we get multi-transition in rare-earth doped fiber is that the depletion of Stark sublevels is selective and depends on the polarization of wave and orientation of ion-dipoles; this is what we already mentioned as hole burnings (spatial, spectral). To increase the inhomogeneity one can cool Er^{+3} doped fiber at liquid nitrogen temperature [26-29]. Generally, in order to produce the multiwavelength fiber laser system we have to employ an intracavity filter. Some researchers propose using the strain gradient of a sampled chirped fiber Bragg grating, integrated in laser ring cavity [30]. In some other works multiwavelength operation of EDF laser has been demonstrated using a polarization controller in ring cavity with which we can also change both the number of lasing lines and spacing between them[31].

1.8 High power fiber laser

High power fiber laser sources with very narrow line width in 1.5 - 1.6 μm spectral region is of great interest in many scientific and engineering applications such as wavelength conversion using Raman fiber lasers[32] and coherent combination[33]. After the first reports on high power fiber laser [34] considerable amount of work has been done to develop such lasers [35,36,37]. Single mode high power fiber lasers are available from 5 watts to greater than 1 kilowatt. These lasers operate in either continuous wave (CW) or pulsed regime at frequencies up to 50 kHz . The laser has application in printing, ranging, and marking [38, 39]. To produce high output power from a laser, we need high power pump Laser and excellent conversion of pump energy to signal power.

1.8.1 Double clad fibers

The output power of the laser can be increased by increasing input pump power or by increasing the interaction between pump and active ions at constant input pump power. To couple high power pump into doped fiber core, we need higher NA of fiber which can be increased by increasing the core diameter or using double clad fiber [40]. Increasing the core diameter in order to get the maximum portion of input pump has some disadvantages like losing the quality of light, transition from single mode to higher modes which leads to some problems such as diffraction loss or degradation in the spatial coherency. Considering all these drawbacks, instead of increasing the core area, researchers use double cladding in order to couple pump light into core. So, the second cladding guides the pump light which gives higher interaction of active ions with pump compared with a single clad fiber with the same core NA as double clad's. Geometrically, the cross section of most fibers are circular. The disadvantage of such kind of shape is that the skew rays never cross the centre of fiber, they always travel on the side of fiber which makes less light interaction with dopants inside the fiber which is a great loss to high power lasers. To overcome this problem either the core should be centrally off in first cladding (for circular cross section fibers) in order to meet the skew rays or if we want to use the centrally placed core, the geometry of first cladding should be different from circular [41,42].

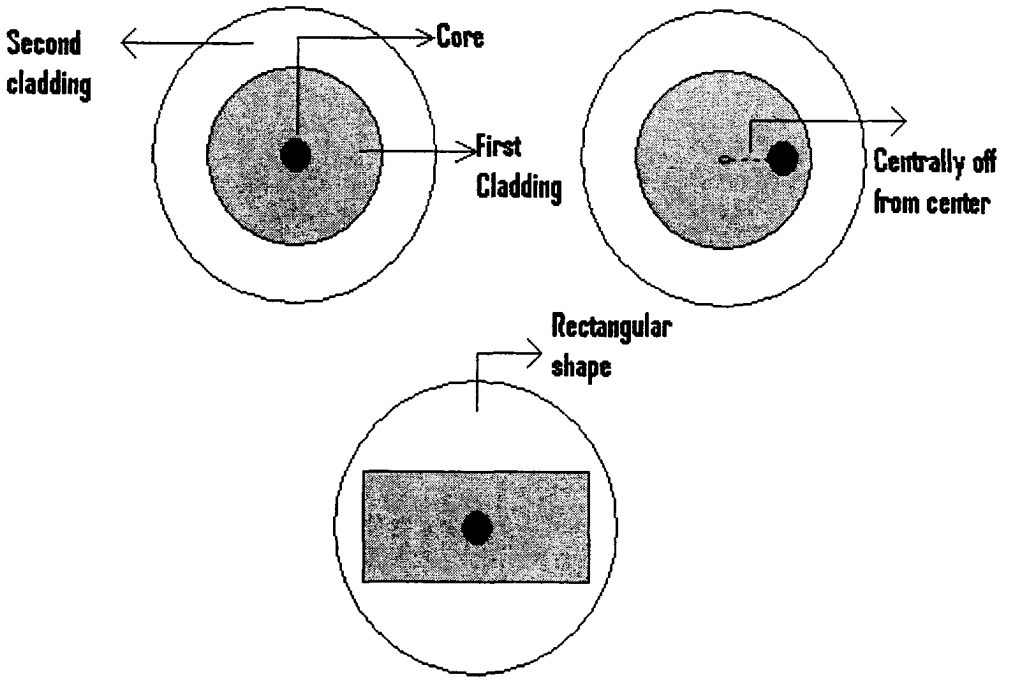

Figure 1.11 Different Cross-Sectional Configuration of Double Clad Fibers

The ratio of absorbable power to pump power is defined as

$$\mu = \frac{P_a}{P_T} \tag{1.30}$$

For circular double clad fibers [41]

$$\mu_1 = \frac{2}{\pi}\left(\frac{\rho}{R_0}\sqrt{1-\left(\frac{\rho}{R_0}\right)^2} + Sin^{-1}\left(\frac{\rho}{R_0}\right)\right) \tag{1.31}$$

ρ and R_0 are the radius of core and first cladding respectively. And for off-set double clad fiber

$$\mu_2 = \frac{2}{\pi}\left(\frac{\rho+P}{R_0}\sqrt{1-\left(\frac{\rho+P}{R_0}\right)^2} + Sin^{-1}\left(\frac{\rho+P}{R_0}\right)\right) \tag{1.32}$$

where P is the offset. Comparing μ_1 and μ_2 we can conclude that because of "P", we

always have $\mu_2 > \mu_1$ and briefly, the larger the P the higher the absorption. But including the rectangular inner cladding with appropriate NA we still get the maximum launched pump power into double clad fibers compared to μ_2 and μ_1.

1.8.2 Er^{3+}-Yb^{3+} Doped fiber

As mentioned earlier a double clad fiber increases the coupling efficiency of the pump laser. Since Er^{+3} has low absorption cross section we can increase its concentration in glass. But at high erbium concentration, some Er^{+3} cluster would be formed[43,44], which cause the ion-ion interaction among Er^{+3} ions resulting in depletion of erbium metastable level. So we can assist to pump Er^{+3} by resonance transfer of energy (Sensitization of Fluorescence) from Yb^{+3}. Due to high absorption cross section of Yb^{+3} ions they absorb appreciable amount of excitation energy and then transfer that to Er^{+3} [45].

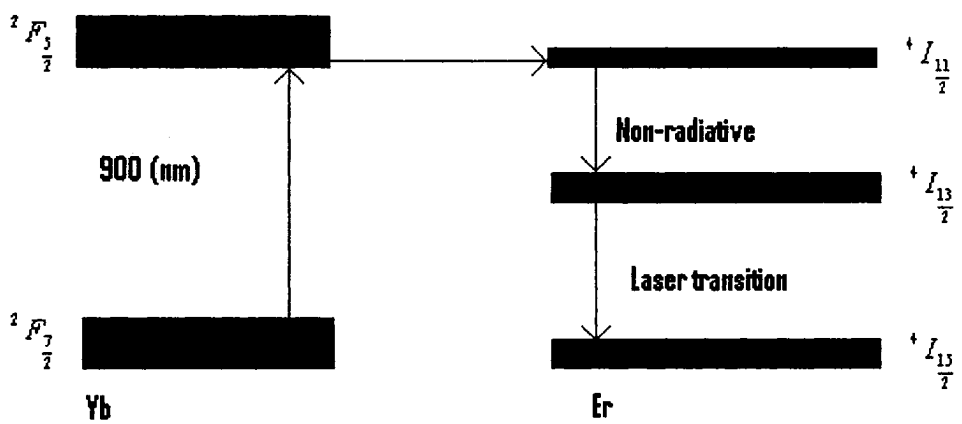

Figure 1.12 Principle of energy transfer between Yb^{+3} and Er^{+3}

In this way we can provide an efficient indirect pumping mechanism for erbium as well as avoid the formation of Er^{+3} clusters by the presence of Yb^{+3}.

1.8.3 High-power multiwavelength fiber laser (HPMWFL)

To produce high power multiwavelength fiber laser, we can use the same technique which we applied before for generating low power multiwavelength fiber laser such as using intracavity filters in a ring cavity [46,47]. In order to produce high output power, we need higher pump conversion efficiency in dopant ions for which, as mentioned before, we can take advantage of resonance transfer of energy between Yb^{+3} and Er^{+3}. Also we need larger modal area to launch the multi mode pump power into core, where cladding pump technique in a double clad fiber is an appropriate solution. Moreover, in efficient cladding pump of $Er^{+3}-Yb^{+3}$ co-doped fiber, we can improve the overlap between modes and active ions by twisting the doped fiber in a figure of eight or kidney shape in which the resulting absorption is almost three to four times more[48] . Other technique to achieve high power multiwavelength fiber laser is to use $Er^{+3}-Yb^{+3}$ co-doped fiber [49]; spatial mode beating filter where a multimode fiber acts as a filter[47].

1.9 Objective

The objective of the proposed research is to design a medium power single-mode multiwavelength fiber laser.

1.10 Organization of the thesis

Chapter 2 describes multiwavelength fiber laser using a Fabry-Perot resonator where an erbium-doped fiber is bidirectionally pumped. Furthermore, we study applicability of Sagnac loop filter in adjusting the separation of lasing lines.

Chapter 3 describes a multiwavelength fiber ring laser using Sagnac loop interferometer as filter. A dynamic grating based on saturable absorber is used as tracking filter to stabilize the lasing lines.

Chapter 4 describes future work.

References:

1- K.C Kao and G. A. Hockam , "Dielectric fiber surface waveguide for optical frequencies," Proc.IEE, vol.113, no.7, pp.1151-1158,1966.

2- C. Randy Giles ,E. Desurvire , "Modeling Erbium-doped fiber amplifiers," J. Lightwave Technol., vol. 9, no.2, pp.271-283, 1991.

3- A.W.Snyder,W.R.Young, "Modes of optical waveguides," J. Opt. Soc. Am., vol.68,no.3,pp.297-309,1978.

4- A.K. Ghatak, K.Thyagarajan , "Optical Electronics,"Cambridge, ch.13, 1989.

5- A.W. Snyder and J.D. Love , "Optical Wave guide Theory," Kluwer Academic, ch.12, 2000.

6- D. Gloge , "Weakly guiding fibers," Appl. Opt., vol.10, no.10, pp.2252-2258, 1971.

7- M. Ohashi , N. Kuwaki , N. Uesugi, " Suitable definition of mode field diameter in view of splice loss evaluation," J. Lightwave Technol., vol. LT-5 ,no.12, pp.1676-1679, 1987.

8- D. Marcuse, " Loss analysis of single – mode fiber splices" , Bell Syst . Technol. J., vol.56,pp. 703-718,1977.

9- D. Gloge, "Dispersion in weakly guiding fibers," Appl. Opt. , vol.10, no.11, pp.2442-45,1971.

10- A.H.Liang , "Transmission characteristics related to Laplacian mode-field half-width of noncircular single-mode waveguides," Appl. Opt., vol.36, no.16,pp.3793-3801, 1997.

11- A.W. Snyder and J.D. Love, "Optical wave guide theory," Kluwer Academic, pp.355-357, 2000.

12- N. Shibata , M. Tokuda , "Measurements of stress profiles in the perform of a polarization –holding fiber with stress-applying parts," J. Light wave Technol., vol. LT-2 , no.3, pp.228,1984.

13- M.P. Varnham , D.N. Payne, A.J. Barlow, R.D. Birch , "Analytic solution for the birefringence produced by thermal stress in polarization-maintaining optical fibers," J. Lightwave Technol. vol.LT-1, no.2,pp.332-339, 1983.

14- J.L. Wagener ,D. G.Falquier , M.J.F. Digonnet and H.J. Shaw, "A muller matrix formalism for modeling polarization effects in Erbium-doped fiber," J. Light wave technol. vol.16, no.2,pp.200-206, 1998.

15- D. Falquier , D. Lande , J.L. Wagener, M.J.F. Diggonet and H.J. Shaw, "Measurements and modeling of The output polarization of Er-Doped fiber lasers," SPIE, Doped fiber Devices and systems, vol.2289, pp.24-38,1994.

16- Born and Wolf, "Principles of Optics," 7^{th} (Expanded) edition ,Cambridge, pp.619-628, 1999

17-P.Myslinski,C.Barnard, X. Pan, Q. Wu and J. Chrostowski , "Applications of rare-earth-doped Fibers," IEEE conference record, Instrumentation and measurement technology conference (IMTC), 193, pp.290-294, 1993.

18- E. Desurvire , "Erbium doped fiber amplifiers," John Wiley & Sons, pp.216-332 ,1994.

19- I.M. Jauncey, L.Reekie,J.E.Townsend,D.N.Payne "Single longitudinal mode operation of an ND^{3+} dopped fiber laser," Electron. Lett.,vol. 24, no.1,pp.24-6, 1988.

20- I.M. Jauncey,L.Reekie,R.J.Mears "Narrow-linewidth fiber laser operating at 1.55 μm," Opt. Lett.,vol.12, no.3, pp.164-65, 1987.

21- G.A.Ball,W.W.Morey "Continuously tunable single mode erbium fiber laser," Opt. Lett., vol.17, no.6, pp.420-22, 1992.

22- G.A.Ball,W.W.Morey,W.H.Glenn "Standing wave monomode erbium fiber laser," IEEE Phton.Technol..Lett. ,vol.3, no.7, pp.613-15, 1991.

23- G.A.Ball,W.H.Glenn, "Design of a single mode linear cavity erbium laser utilizing bragg reflector," J. Lightwave Tech.,Vol.10,No.10, pp.1138-43, 1992.

24- J.L.Zyskind,J.W.Sulhaff,Y.Sun,J.Stone,L.W.Stalz,G.T.Harvey,D.J.DiGiovanni, H.M. Presby,A.Picci rilli,U.Koren,R.M.Jopson, "Single mode diode pumped tunable erbium doped fiber laser with linewidth less than 5.5 KHz," Electron. Lett.,vol.27, Page 2148, 1991.

25- J.J.Pan,Yuan Shi, "Tunable Er^{3+} doped fiber ring laser using fiber grating incorporated by optical circulator or fiber coupler," Electron. Lett. , vol.31, no.14, pp.1164-65,1995.

26- N.Park,P.F.Wysocki ,"24-line multi wavelength operation of erbium doped fiber ring laser,"IEEE Photon.Technol.Lett., vol.8, no.11,pp.1459-61,1996.

27- J.Chow,G.Town,B.Eggleton,M.Ibsen Sugden,Ian Bennion, "Multiwavelength generation in an erbium doped fiber using in fiber comb filters," IEEE Photon .Technol.Lett., vol.8, no.1,pp.60-62,996

28- H.L.An,X.Z.Lin,E.Y.B.Pun,H,D.Liu, "Multiwavelength operation of an erbium doped ring laser using a dual pass Mach-Zehnder comb filter," Opt. Commun., vol.169,pp.159-65,1999.

29- X.Shu,S.Jiang,D.Huang, "Fiber grating Sagnac loop and its multiwavelength laser application,"IEEE Photon.Technol.Lett.,vol.12, no.8,pp. 980-983, 2000.

30- J.Yang,S.C. Tjin,N.Q.Ngo, "Multiwavelength tunable fiber ring laser based on sampled chirp fiber bragg gartin," IEEE Photon.Technol. Lett. ,vol.16,no.4, pp.1026-28, 2004.

31- L.Zhihong,L. Caiyun,G.Yizhi ,"A Polarization controlled multiwavelength Er-doped fiber Laser," Fifth Asia-Pacific Conference, pp.1506-08 ,1999.

32- Ming Tang; Yandong Gong; Ping Shum, "Broad-band tunable wavelength conversion using Raman-assisted parametric four-wave mixing in highly nonlinear fibers with double -pass Geometry," IEEE Photon.Technol. Lett.,vol.17, no.1, 2005.

33- B.He,Q.Lou,J.Zhou,J.Dong,Y.Wei,D.Xue,Y.Qi,Z.Su,L.Li,F.Zhang, "High power coherent beam combination from two lasers,"Opt. Express, vol.14, no.7,2006.

34- V.P.Gapontsev,I.E.Samartsev ,"High power fiber lasers," OSA Proceedings on advanced solid state lasers,vol.6, pp.258-262, 1990.

35- Y. Jeong , J.K. Sahu , D.B.S. Soh , C. A . Codemard , and J. Nilsson, "High-power tunable single-frequency single-mode erbium: ytterbium codoped large-core fiber master-oscillator power amplifier source," Opt. Lett., vol.30, no. 22, pp.2997-99, 2005.

36- Reichel, Volker, Moerl, Klaus W.; Unger, Sonja; Jetschke, Sylvia; Mueller, Hans-Rainer; Kirchhof, Johannes; Sandrock, Thomas; Harschack, Alexander; Liem, Andreas; Limpert, Jens;Zellmer, Holger; Tuennermann, Andreas "Fiber-laser power scaling beyond the 1-kilowatt level by Nd:Yb co-doping;SPIE, Int. Soc. Opt. Eng.,WA 98227-0010(2005).

37- Y. Jeong, J.K. Sahu, D.N. Payne, and J. Nilsson, "Ytterbium-doped large-core fibre laser with 1 kW of continuous-wave output power," Electron. Lett.,vol.40 , pp.470-2, 2004.

38- Z.G. Lu, F.G. Sun, G.Z. Xiao, P. Lin and P. Zhao , "High-power multi wavelength Er^{+3}-Yb^{+3} codoped double-cladding fiber ring laser," IEEE. Photonics Technol. Lett. ,vol . 17,no.9, pp.1821- 23, 2005.

39- N.S.Platonov,D.V.Gapontsev ,"135W CW fiber laser with perfect single mode output,"CPDC3-1/3.

40- S.Bedo , W. Luthy ,H.P. Weber , "The effective absorption coefficient in double-clad fibers," Opt. Commun., 99 ,pp. 331-335,1993.

41- A. Liu ,K. Ueda, "The absorption characteristics of circular ,offset and rectangular double-clad Fibers," Opt. Commun., 132, pp. 511-518,1996.

42- D. Kouzenetsov, J.V. Moloney, "Efficiency of pump absorption in double-clad fiber amplifiers," J. Opt. Soc. Am. B, vol.19, no.6, pp.1259-63, 2002.

43- P. Myslinski, D.Nguyen, J.Chrostowski, "Effects of concentration on the performance of Erbium-doped fiber amplifier,"J.Lightwave Technol.,vol.15, no.1, pp.112-20,1997.

44- M.R.X. de Barros, G. Nykolak, D.J. DiGiovanni, A. Bruce,W.H. Grodkiewicz, P.C. Becker, "Performance of a high concentration Er/sup 3+/-doped alumino silicate fiber amplifier," IEEE Photon.Technol.Lett.,vol.8,no.6, pp.761-63,1996.

45-W.L. Barnes ,S.B. Poole , J.E. Townsend , L. Reekie ,D.J. Taylor and D.N. Payne , "Er^{+3}-Yb^{+3} and Er^{+3} doped fiber lasers," J. Lightwave Technol., vol.7, no.10, pp.1461-65, 1989.

46- I.Torres-Gomez,A.Martinez-Rios,G.Anzueto-Sanchez,R.Selvas-Aguilar,A. Martinez-Games,D.Monzon-Hernandez, "Multi-wavelength switchable double clad Yb^{+3}-doped fiber laser based on reflectivity control of fiber brag gratings by induced bend loss" Opt.Rev.,vol.12,no.2,pp.65-68,2005.

47- Z.G.Lu,F.G.Sun,G.Z.Xiao,P.Lin,P.Zhao ,"High power multi wavelength Er^{+3}-Yb^{+3} codoped double cladding fiber ring laser,"IEEE Photon.v Technol. Lett., vol.17, no.9, pp.1821-23, 2005.

48- Chen Z.J., Minelly J.D.,Dong L.,Vienne G.G.,Payne D.N. ,"Effiecient cladding pumped Er/Yb doped fiber amplifier and bending effect in cladding pumping scheme,"CLEO Europe 96,CTHL3(1996).

49- Loh W.H., Morkel P.R., Payne D.N. ,"Wavelength selection and tuning by optical control in a two-segment erbium-doped fiber laser," vol.6,no.1, pp.43-46, 1994.

Chapter 2

A multiwavelength fiber laser using bidirectional pumping method for producing high power Laser

2.1 Introduction

High power and narrow line width fiber lasers have attracted much attention due to their applications in sensors, spectroscopy, and optical communications. In this chapter we describe a multiwavelength fiber laser using bidirectional pumping method of an erbium-doped fiber in FP resonator configuration. We also investigated the application of a Sagnac loop interferometer as a tunable filter. Efficient coupling of high power from pump laser into rare earth-doped fiber is one of the challenging tasks of designing a high power fiber laser. As mentioned earlier (chapter 1, section 1.8.1), cladding pumped $Er^{+3} - Yb^{+3}$ doped fiber is a preferred choice for high power fiber laser where the pump power is carried by the cladding (Figure 2.1). The slope efficiency of the pump absorption for cladding pumping is 38 percent more compared to single clad rare-earth doped fiber pumping [1]. There are different methods to pump the doped fiber such as

Side Pumping [2], Cladding Pumping by Fiber Bundles [3] and Bidirectional pumping[4]. The configurations of unidirectional (forward) and bidirectional pumping are shown in Figure2.2 .

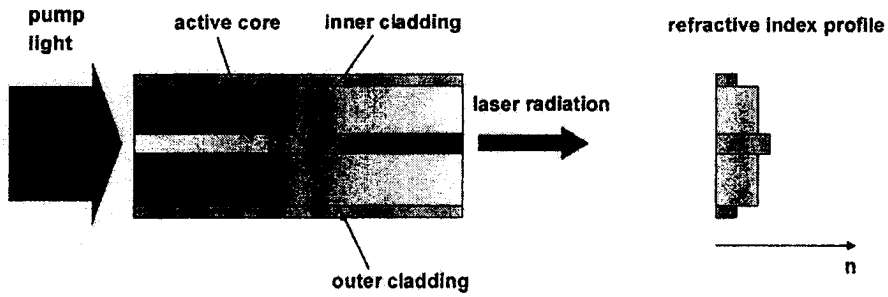

Figure 2.1 cladding pumped fiber

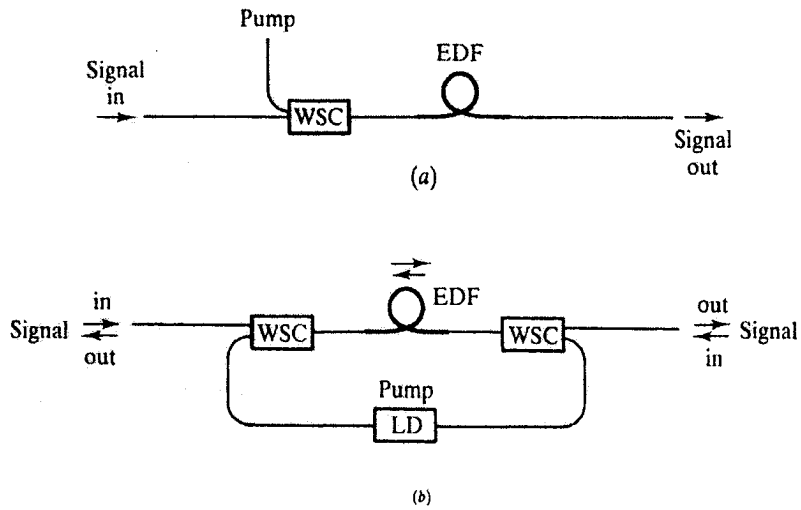

WSC : wavelength selective coupler

Figure 2.2 (a) Standard forward pumping (b) Bidirectional pumping

The experimental and theoretical studies shows bidirectional pumping is more efficient than unidirectional one[5]. In bidirectional pumping for single clad active fiber

more active ions inside the core interact with pump power so optimum length of fiber in order to get particular gain is less than forward pumping with the same pump power.

2.2 Theory

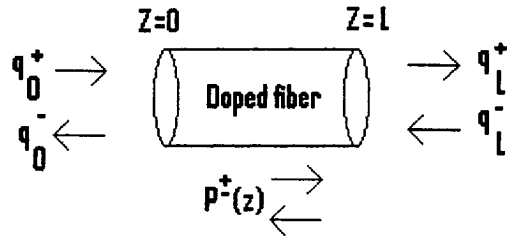

Figure 2.3 Bidirectional pumping

In an amplifier, for a doped fiber of length L the relation between the normalized input (q_0^+, q_L^-) and output (q_L^+, q_0^-) pump powers at $z = 0, L$ (Figure 2.3) in bidirectional pumping method [6,7] is given by,

$$q^{\pm}(z) = \frac{P_p^{\pm}(z)}{P_{sat}^{*}(\lambda_p)} \tag{2.1}$$

and

$$P_{sat}^{*}(\lambda_p) = \frac{h\nu_p A_{eff}}{(\sigma_a(\lambda_p) + \sigma_e(\lambda_p))\tau} \tag{2.2}$$

where

$P_{sat}^{*}(\lambda_p)$ = effective pump saturation power

$\sigma_{a,e}(\lambda_p)$= absorption and emission cross section

$\tau = {}^4I_{\frac{13}{2}}$ fluorescence life time $\approx 10\ ms$

A_{eff} = effective pump area

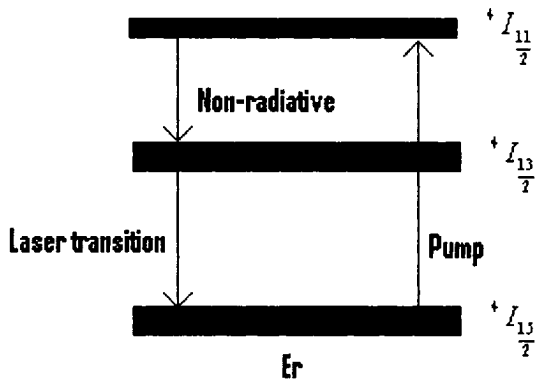

Figure 2.4 Pump and Laser transition

If $p^{\pm}(z) = \frac{P_k^{\pm}(z)}{P_{sat}^{*}(\lambda_k)}$ be the forward and backward normalized signal powers at "z",

where $P_{sat}^{*}(\lambda_k)$ is the effective signal saturation power, then the equation related to the gain and input pump powers q_0^{+}, q_L^{-} [7] is,

$$q_0^{+} + q_L^{-} = \frac{b}{2}\frac{\exp(A_{pk}L)}{\exp(-wL)-1}\left((1+\exp(-A_{pk}L))(1-\exp(-wL)) - (1-\exp(-A_{pk}L))(1+\exp(-wL))\sqrt{1-4\frac{q_0^{+}q_L^{-}}{b^2}}\right)$$

$$A_{pk} = \alpha_p \frac{1+\eta_p}{1+\eta_k}\left((1+\varepsilon_k)(1-bc)\varepsilon_p - \frac{\log G_k}{\alpha_k L}\right) \qquad (2.3)$$

$$q_L^{\pm} = q_0^{\pm}\exp(-A_{pk}L)$$

where

A_{pk} = Gain dependent pump

$$\varepsilon_{k,p} = \frac{\alpha'_{k,p}}{\alpha_{k,p}}$$

$\alpha_{k,p}$ and $\alpha'_{k,p}$ = fiber background absorption and Er^{+3} absorption coefficient at $\lambda_{k,p}$ respectively

$$\eta_{p,k} = \frac{\sigma_e(\lambda_{p,k})}{\sigma_a(\lambda_{p,k})}$$

Similarly, the relation between signal and amplifier gain, $G(q)$ is,

$$p_k^{\pm}(q_{L,0}^{+}) = G_k^{+}(q_{L,0}^{+})\left(p_k^{\pm}(q_{0,L}^{+}) + p_0 \frac{\alpha_s}{\alpha'_s}\frac{\eta_k}{1+\eta_p}\int_{q_L^{+}}^{q_0^{+}} \frac{(a+x^2)dx}{x(a+bx+x^2)G_k^{\pm}(x)} \right) \qquad (2.4)$$

In Equation 2.4 the first term in braces is amplified signal and the second term corresponds to amplified spontaneous emission. Since amplified spontaneous emission noise is due to the incomplete erbium inversion and the effect of insufficient pump absorption by Erbium ions, by using bidirectional pumping we enhance the erbium ions absorption which results in giving the advantage of more uniform population inversion along the fiber and increase of gain coefficient. The total pump power $(q_0^{+} + q_L^{-})$ required for transparency in bidirectional pumped Er-doped fiber as a function of absorption coefficient is shown below ;

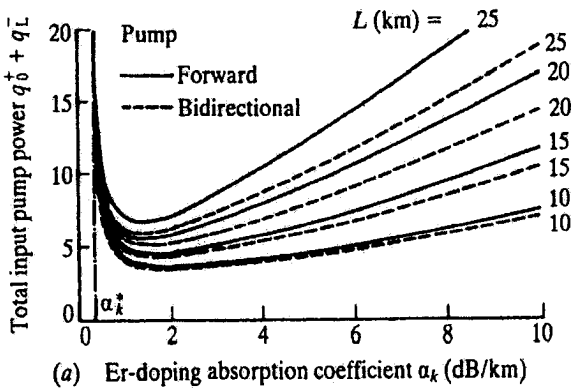

Figure 2.5 The normalized pump power Vs. Er. Absorption coefficient for different fiber length [6]

2.3 Sagnac loop filters

A simple technique to construct a multiwavelength laser source is to use a broadband gain medium together with an optical filter to select lasing wavelengths [8,9,10,11]. A Sagnac loop interferometer [12] is widely used for producing multiple peaks in designing multiwavelength fiber laser. It consists of 3 dB fiber coupler , polarization maintaining fiber(PMF) and a polarization controller (PC). Figure 2.6 shows the schematic of the Sagnac loop. It exhibits low insertion

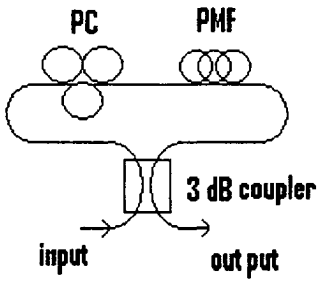

Figure 2.6 Sagnac loop interferometer

loss, polarization independence to input light and high resistance to environmental changes, because both counterpropagating light waves travel the same optical path before recombining at the fiber coupler. These characteristics make it a promising wavelength-selective tool for multiwavelength fiber lasers. Besides, if polarization maintaining fiber is affected by environmental changes such as temperature, it results in just a slow drift of the transmission wavelengths. By adjusting polarization controller plates we can shift the output spectrum of the Sagnac loop interferometer. The filter spacing can be adjusted by changing the length of polarization maintaining fiber or by cascading different length of polarization maintaining fiber to change the effective length of birefringence fiber[13].

One of the main tasks in this thesis is to study, both theoretically and experimentally, the application of Sagnac loop interferometer inside a FP or ring resonator.

2.3.1 Sagnac loop filter using single-segment polarization - maintaining fiber

Using Jones Matrix method we can find out the transmission and reflection function of the Sagnac loop interferometer for a particular length of PMF [14-16]. Denoting $E_{x,y}^{T}, E_{x,y}^{In}$ as X - Y components of input and transmitted fields with wavelength of λ and $\delta = \frac{2\pi BL}{\lambda}$ phase retardance of PMF, where "L" is the length of the PMF and "B" is the birefringence. For fast axis rotation angle θ, the Jones matrix for the light in clock-wise direction (Figure 2.7) is ,

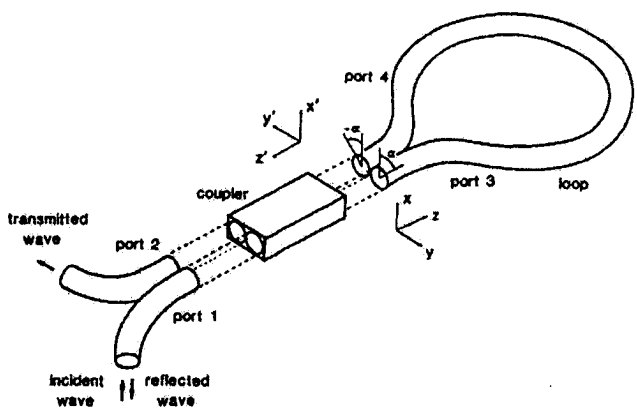

Figure 2.7 System of axis required to express the Sagnac loop analysis ($\alpha = \theta$)

$$M(\theta) = \begin{bmatrix} Cos\left(\frac{\delta}{2}\right) + i\,Sin\left(\frac{\delta}{2}\right)Cos(2\theta) & i\,Sin(2\theta)Sin\left(\frac{\delta}{2}\right) \\ i\,Sin(2\theta)Sin\left(\frac{\delta}{2}\right) & Cos\left(\frac{\delta}{2}\right) - i\,Sin\left(\frac{\delta}{2}\right)Cos(2\theta) \end{bmatrix} = \begin{bmatrix} A & B \\ -B^{*} & A^{*} \end{bmatrix} \quad (2.5)$$

similarly the Jones matrix for light beams traveling the loop in counter-clock wise direction is

$$M(-\theta)=\begin{bmatrix} A & B^* \\ -B & A^* \end{bmatrix} \tag{2.6}$$

and the transmission coefficient is

$$t=\frac{\overline{E}^T}{\overline{E}^{In}}=\frac{1}{2}[M(\theta)-M(-\theta)] \tag{2.7}$$

or

$$\begin{bmatrix} E_x^{\ T} \\ E_y^{\ T} \end{bmatrix}=\frac{1}{2}[M(\theta)-M(-\theta)]\begin{bmatrix} E_x^{\ In} \\ E_y^{\ In} \end{bmatrix}$$

Finally the transmission function $T(\lambda)$ is,

$$\frac{\left|\overline{E}^T\right|^2}{\left|\overline{E}^{In}\right|^2}=T(\lambda)=Sin^2(2\theta)\,Sin^2\left(\frac{\delta}{2}\right) \tag{2.8}$$

Adjusting the PC plates in loop, we can make $\theta=\frac{\pi}{4}$ and thus Equation 2.8 reduces to

$$T(\lambda)=Sin^2\left(\frac{\delta}{2}\right) \tag{2.9}$$

where maximum transmission occurs at $\delta=(2n+1)\pi \quad n=0,1,2,3...$ and the spacing $(\Delta\lambda)$ between two transmission maxima is

$$\Delta\lambda = \frac{\lambda^2}{BL} \tag{2.10}$$

So, in order to change the spacing we have to change length of the PMF or birefringence.

2.3.2 Sagnac loop filter using 2-segment polarization-maintaining fiber

As mentioned earlier, in order to have different transmission spectrum with different spacing, we should change the effective length of PMF inside the loop. It is possible to change effective length of PMF using multiple segments of PMF inside the Sagnac loop filter [13].

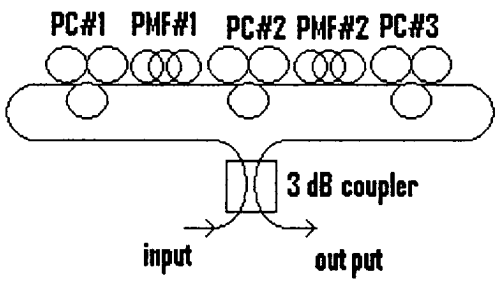

Figure 2.8 2-segment PMF Sagnac loop

As shown in Figure 2.8 we used a Sagnac loop comprising two pieces of PMF and three PCs' successively. Following the same procedure as for one-segment PMF Sagnac loop and considering the effective birefringence matrix for two-segment PMF as

$M(\theta)$, where

$$M(\theta) = M_2(\theta_2)M_1(\theta_1) \tag{2.11}$$

and likewise $M(-\theta)$

$$M(-\theta) = M_1(-\theta_1)M_2(-\theta_2) \tag{2.12}$$

the transmission function is,

$$T(\lambda) = \left[Sin(2\theta_2)\, Sin\left(\frac{\delta_2}{2}\right) Cos\left(\frac{\delta_1}{2}\right) + Sin(2\theta_1)\, Sin\left(\frac{\delta_1}{2}\right) Cos\left(\frac{\delta_2}{2}\right) \right]^2 \tag{2.13}$$

where θ_1, θ_2, δ_1, δ_2 are fast axis rotation and phase retardance for each PMF piece, respectively. By adjusting the PCs we can get two different transmission spectrums,

i. $\theta_1 = \frac{\pi}{4}$ & $\theta_2 = \frac{\pi}{4}$ $\Rightarrow T(\lambda) = Sin^2\left(\frac{\delta_1 + \delta_2}{2}\right)$ (2.14)

ii. $\theta_1 = \frac{\pi}{4}$ & $\theta_2 = -\frac{\pi}{4}$ $\Rightarrow T(\lambda) = Sin^2\left(\frac{\delta_1 - \delta_2}{2}\right)$

So, comparing these results with what we calculated earlier for one-segment PMF Sagnac loop filter we can express BL in Equation 2.10 as ,

$$(BL)_{eff} = B_1L_1 \pm B_2L_2 \tag{2.15}$$

and

$$\Delta\lambda = \frac{\lambda^2}{B_1L_1 \pm B_2L_2} \tag{2.16}$$

Thus, by using 2-segment PMF we can produce two different spectrum.

2.3.3 Sagnac loop filter using 3-segment polarization-maintaining fiber

Following the same procedure to get more flexibility of changing wavelength

spacing we considered a Sagnac loop comprising three segments of PMF and four individual PCs as shown in Figure 2.9,

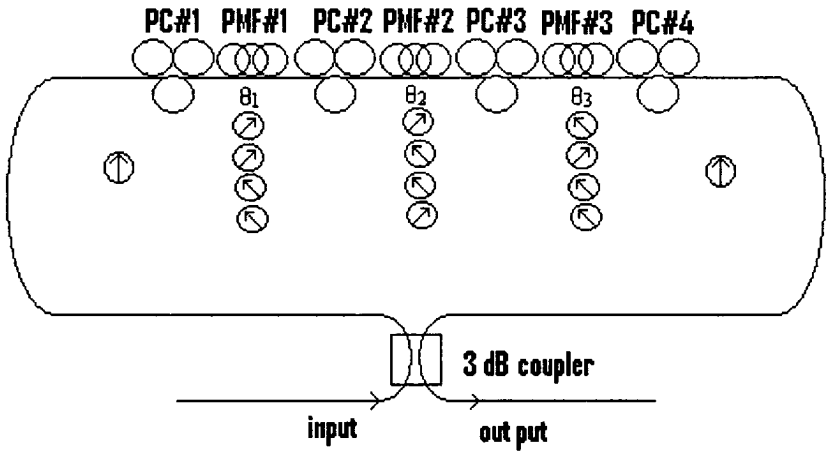

Figure 2.9 3-segment PMF Sagnac loop

considering the effective birefringence matrix for this loop as $M(\theta)$

$$M(\theta) = M_3(\theta_3)M_2(\theta_2)M_1(\theta_1) \tag{2.17}$$

and likewise $M(-\theta)$

$$M(-\theta) = M_1(-\theta_1)M_2(-\theta_2)M_3(-\theta_3) \tag{2.18}$$

we can calculate the transmission function as

(2.19)

$$T = \left[\begin{array}{l} -\left(Sin(2\theta_1)Sin(2\theta_2)Sin(2\theta_3)Sin\left(\frac{\delta_1}{2}\right)Sin\left(\frac{\delta_2}{2}\right)Sin\left(\frac{\delta_3}{2}\right)\right) \\ + Sin(2\theta_1)Sin\left(\frac{\delta_1}{2}\right)\left(Cos^2(\theta_2)Cos^2(\theta_3)\cos\left(\frac{\delta_2+\delta_3}{2}\right) + Sin^2(\theta_2)Sin^2(\theta_3)\cos\left(\frac{\delta_2+\delta_3}{2}\right) + Cos^2(\theta_2)Sin^2(\theta_3)\cos\left(\frac{\delta_2-\delta_3}{2}\right) + Sin^2(\theta_2)Cos^2(\theta_3)Cos\left(\frac{\delta_2-\delta_3}{2}\right)\right) \\ + Sin(2\theta_2)Sin\left(\frac{\delta_2}{2}\right)\left(Cos^2(\theta_1)Cos^2(\theta_3)\cos\left(\frac{\delta_1-\delta_3}{2}\right) + Sin^2(\theta_1)Sin^2(\theta_3)\cos\left(\frac{\delta_1-\delta_3}{2}\right) + Cos^2(\theta_1)Sin^2(\theta_3)\cos\left(\frac{\delta_1+\delta_3}{2}\right) + Sin^2(\theta_1)Cos^2(\theta_3)Cos\left(\frac{\delta_1+\delta_3}{2}\right)\right) \\ + Sin(2\theta_3)Sin\left(\frac{\delta 3}{2}\right)\left(Cos^2(\theta_1)Cos^2(\theta_2)\cos\left(\frac{\delta_2+\delta_1}{2}\right) + Sin^2(\theta_1)Sin^2(\theta_2)\cos\left(\frac{\delta_2+\delta_1}{2}\right) + Cos^2(\theta_1)Sin^2(\theta_2)\cos\left(\frac{\delta_1-\delta_2}{2}\right) + Sin^2(\theta_1)Cos^2(\theta_2)Cos\left(\frac{\delta_1-\delta_2}{2}\right)\right) \end{array} \right]^2$$

Again considering four particular cases for distinct combination rotation angles of three PMF segments $(\theta_1, \theta_2, \theta_3)$ we can simplify the transmission function to,

(2.20)

i. $\theta_1 = \theta_3 = \frac{\pi}{4}; \theta_2 = -\frac{\pi}{4} \quad \Rightarrow T(\lambda) = Sin^2\left(\frac{\delta_1 - \delta_2 + \delta_3}{2}\right)$

ii. $\theta_1 = \theta_2 = \theta_3 = \pm\frac{\pi}{4} \quad \Rightarrow T(\lambda) = Sin^2\left(\frac{\delta_1 + \delta_2 + \delta_3}{2}\right)$

iii. $\theta_1 = \theta_2 = \frac{\pi}{4}; \theta_3 = -\frac{\pi}{4} \quad \Rightarrow T(\lambda) = Sin^2\left(\frac{\delta_1 + \delta_2 - \delta_3}{2}\right)$

iv. $\theta_2 = \theta_3 = -\frac{\pi}{4}; \theta_1 = \frac{\pi}{4} \quad \Rightarrow T(\lambda) = Sin^2\left(\frac{\delta_1 - \delta_2 - \delta_3}{2}\right)$

the effective BL are,

$$(BL)_{eff} = \begin{cases} B_1L_1 + B_2L_2 + B_3L_3 \\ B_1L_1 - B_2L_2 + B_3L_3 \\ B_1L_1 + B_2L_2 - B_3L_3 \\ B_1L_1 - B_2L_2 - B_3L_3 \end{cases} \tag{2.21}$$

In the case of N segments of PMF in Sagnac loop we can expect $2^{(N-1)}$ number of individual effective lengths [17,18] and corresponding transmission spectrum.

2.4 Resonator

Our objective in this research project is to design an efficient resonator for high power multiwavelength fiber laser. Figure 2.10 shows a FP resonator where a bidirectional pumping scheme is used. This resonator comprises of two three-port

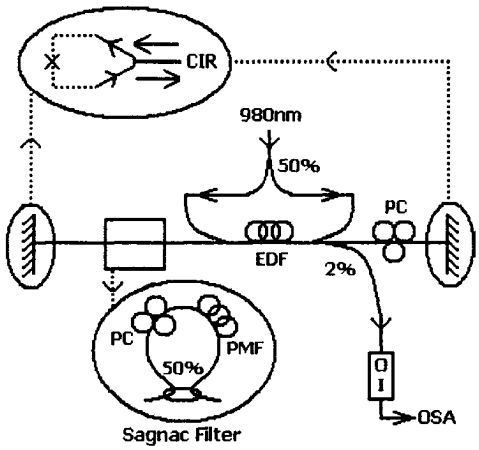

Figure 2.10 Fiber laser resonator [19]

polarization independent circulator (Appendix I) as the mirrors of Fabry-Perot resonator, a Sagnac loop filter, one polarization controller to adjust the polarization of the light inside the cavity and polarization-maintaining erbium-doped fiber as a gain medium which is bi-directionally pumped using a 980 nm laser through two 980/1550 wavelength division multiplexer (Appendix II). The output of this laser is observed by an optical spectrum analyzer of resolution 0.05 nm. In this chapter, we explore the effect of Sagnac loop on the output spectrum, the bidirectional pumping scheme etc.

2.4.1 Theory of the passive resonator

The output of the passive resonator without the Sagnac loop filter shown in Figure 2.11 is given by

$$\frac{I_{out}}{I_{in}} = \frac{T^2{}_2 \exp(-2\alpha L)}{\left(1-\sqrt{R_1 R_2}\exp(-2\alpha L)\right)^2 + 4\sqrt{R_1 R_2}\exp(-2\alpha L)Sin^2(\beta L)} \qquad (2.22)$$

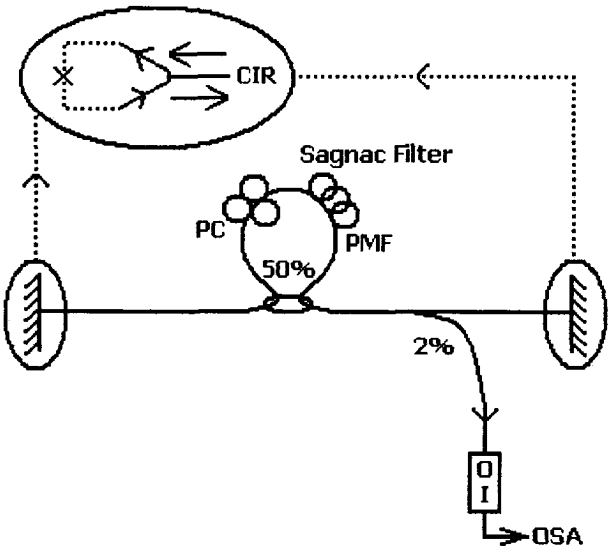

Figure 2.11 Passive Fabry-Perot resonator including Sagnac loop filter

where R_1, R_2, T_2 are the reflectance and transmittance of mirrors and "L" is the length

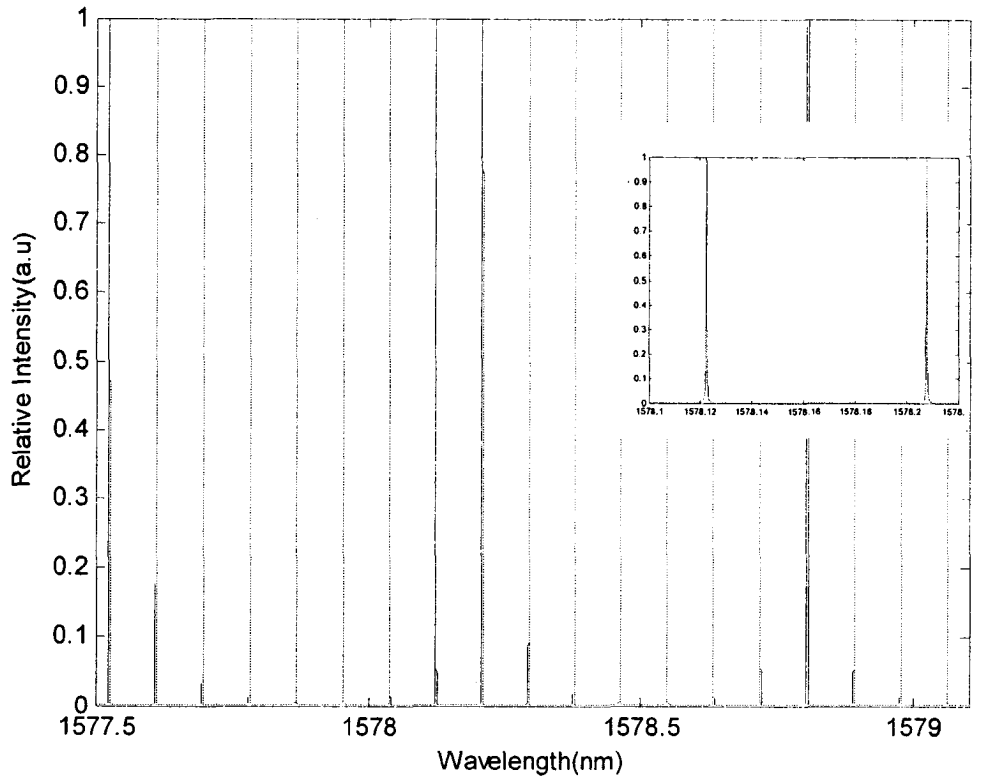

Figure 2.12 Relative Intensity Vs. Wavelength for FPR. L=.01 m , n=1.46,

$R_1 = 1,\ R_2 = 0.98, \alpha = 0, \Delta\lambda = .08nm$; $FWHM = 4 \times 10^{-4}\, nm$

of the cavity and α is total loss of the cavity. Figure 2.12 shows the output of the passive resonator. The Finesse of the resonator is

$$F = \frac{\pi (R_1 R_2)^{\frac{1}{4}} \exp(-\alpha L)}{1 - \sqrt{R_1 R_2} \exp(-2\alpha L)} \tag{2.23}$$

Figure 2.13 shows the transmission spectrum of Sagnac loop filter (Equation 2.9),

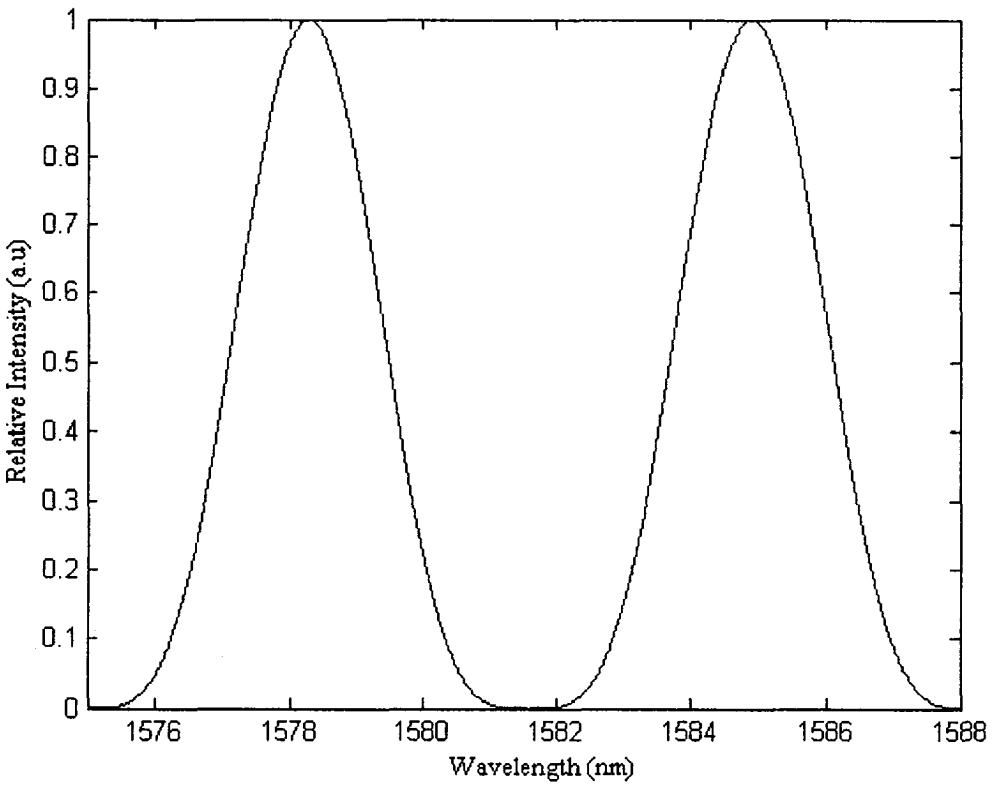

Figure 2.13 Transmission spectrum of Sagnac loop filter ,

$$L_{PMF} = 1\ m, B = 3.7 \times 10^{-4}, (FSR)_{sagnac} = \frac{\lambda^2}{BL_{PMF}} \approx 6.6\ nm$$

the expression for the output of the resonator shown in Figure 2.11 with the Sagnac loop is

(2.24)

$$\frac{I_{out}}{I_{in}} = \frac{T^2{}_2\ Sin^2\left(\frac{\delta}{2}\right)\exp(-2\alpha L_t)}{\left(1-\sqrt{R_1R_2}Sin^2\left(\frac{\delta}{2}\right)\exp(-2\alpha L_t)\right)^2 + 4\sqrt{R_1R_2}\exp(-2\alpha L_t)Sin^2\left(\frac{\delta}{2}\right)Sin^2(\beta L)}\ ;\quad L_t = L_{PMF} + L$$

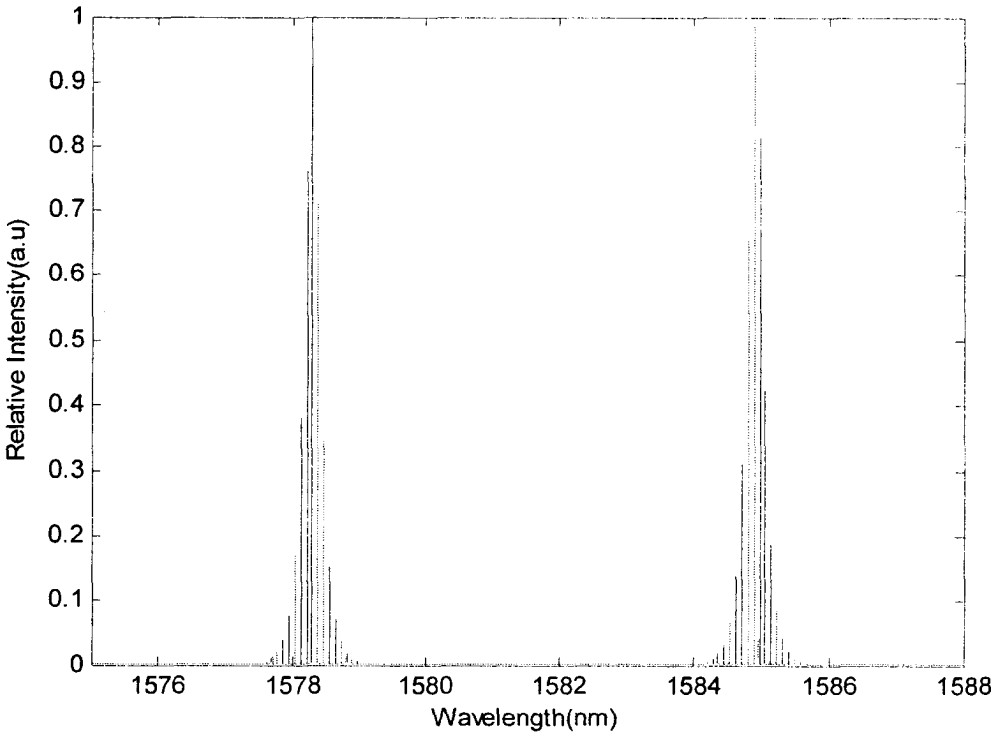

Figure 2.14 Transmission spectrum of the resonator with Sagnac loop inside; $L_{PMF} = 1\ m, B = 3.7\times10^{-4}$

Figure 2.14 shows output of the resonator with a Sagnac loop filter. Comparing Figures 2.12 and 2.13 and 2.14 we can conclude that the transmission spectrum of the resonator is modulated by the transmission function of Sagnac loop filter.

2.4.2 Experimental results

An elliptical core erbium doped fiber of length 3 m and of absorption 18 dB/m at 980 nm is used inside the cavity. In order to justify the function of Sagnac loop in our cavity with theoretical results, we used different lengths of polarization-maintaining fiber in our one segment Sagnac loop. Figures 2.15 (a), 2.15 (b), 2.15 (c), show dual-wavelength fiber laser for polarization-maintaining fiber of lengths 180 cm, 5 m and 8 m respectively.

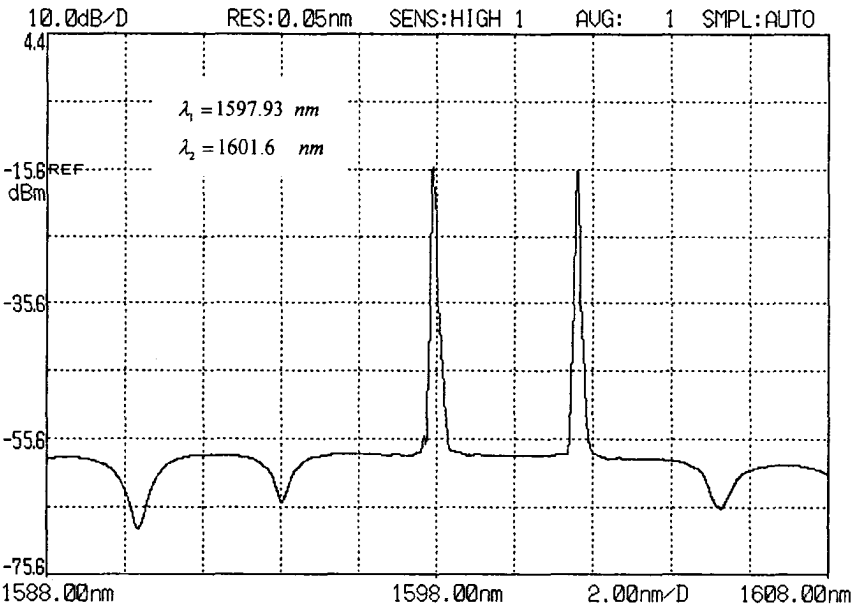

(a)

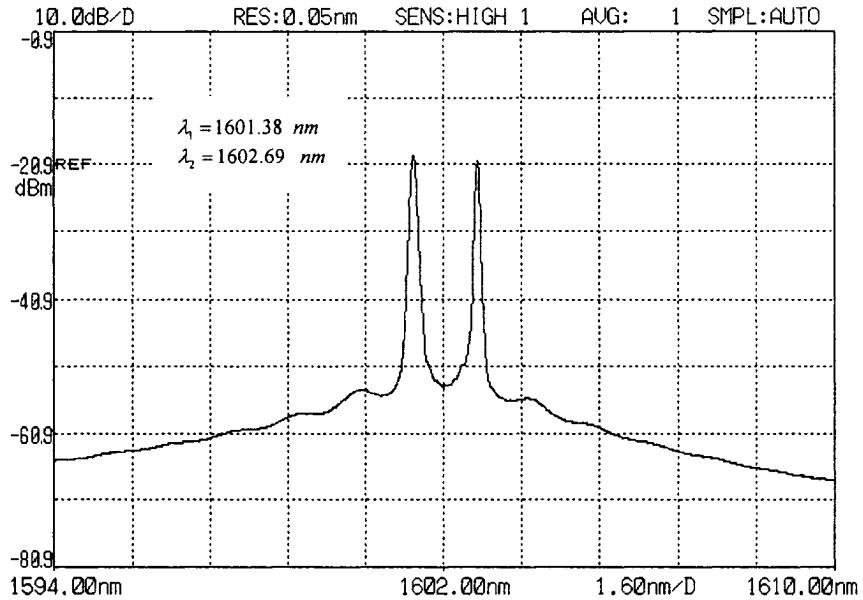

(b)

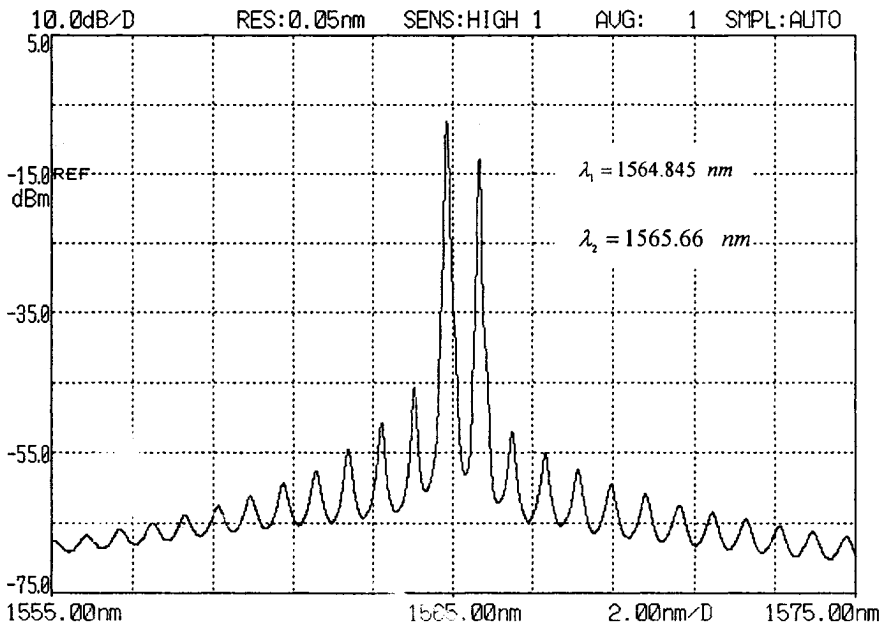

(c)

Figure 2.15 Spectrum of two lasing lines (a) $L_{pmf} = 180\,cm, \Delta\lambda \approx 3.6\,nm$, (b) $L_{pmf} = 5\,m, \Delta\lambda \approx 1.3\,nm$ (c) $L_{pmf} = 8\,m, \Delta\lambda \approx .8\,nm$

2.5 Conclusion

The maximum output power from the laser obtained for an input pump power of ≈ 300 mW is less than 3 mW (Figure 2.16). The multiavelength fiber laser using bidirectional pumping method cannot produce high output power, because of high pump power coupling loss due to core-ellipticity of the doped fiber. The other reason includes unavailability of suitable high power single mode pump laser.

In chapter 3, we design a ring resonator for producing high power multiwavelength fiber laser. A double clad $Er^{+3} - Yb^{+3}$ doped fiber is used as gain medium together with a high power multimode 976 nm pump laser. The output of the laser is more than 100 mW.

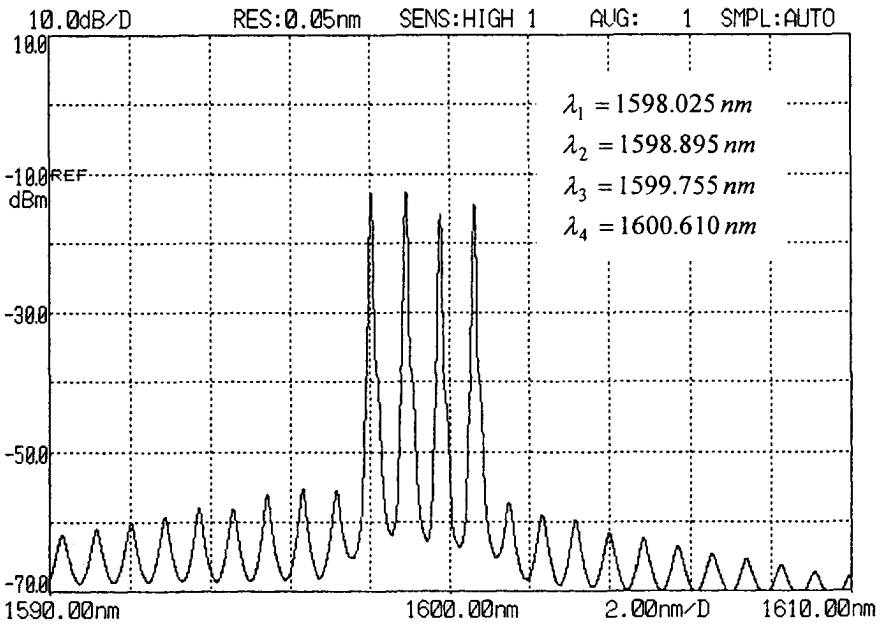

Figure 2.16 Experimental results show that the laser can produce a maximum output power of ≈ 3 mw for an input pump power of ≈ 300 mW , $\Delta\lambda \approx .8\,nm$

References :

1- S.U.Alam , P.W.Turner , A.B.Grudinin, J.Nilson, J.A.Alvarez-Chavez,W.A.Clarkson, "High Power and tunable operation of erbium-ytterbium co-doped cladding pumped fiber lasers," IEEE J.Quantum Electron., vol.39,no.8,pp.987-994,2003.

2- P. Krupka ,A.F.Grobelny,E.M.Beres-Pawlik,J.Wojcik, "Double-clad fiber laser pumping by side coupling method," International Conference on Transparent Optical Networks, pp.213- 216,2004.

3- A. Kosterin,V.Temyanko, M.Fallahi, M.mansuripur, "Tapered fiber bundles for high power applications," Optical Fiber Communication Conference, 2005.

4- S. P. Batien , H. R. D. Sunak, "Comparison of forward and bidirectional pumping at 805 and 819 nm in Er-Doped Silica fiber amplifiers," IEEE Photon. Technol.Lett.,vol.3,no.5,pp.456-8,1991.

5- S.P.Chen,K.Lu,J.Li, "Bidirectionally pumped spectrum-presliced multiwavelength fiber source with a double-pass Mach-zender interferometer,"Opt. Eng.,vol.44,no.8,pp.1-5,2005.

6- D.N.Chen and E.Desurvire , "Noise performance evaluation of distributed Erbium-Doped amplifiers with bidirectional pumping at 1.48 micrometer," IEEE Photon. Technol.Lett.,vol.4,no.1,pp.52-55, 1992.

7- E. Desurvire ,"Erbium-doped amplifiers,Principle and applications," John Wiley,ch.1,2,6 Appendix E,1994.

8- J.Yang,S.C. Tjin,N.Q.Ngo, "Multiwavelength tunable fiber ring laser based on sampled chirp fiber bragg gratin," IEEE Photon.Technol. Lett. ,vol.16,no.4, pp.1026-28, 2004.

9- S.Yamashita,K.Hsu,W.H.Loh, "Miniature Erbium:Ytterbium fiber Fabry-Prot multiwavelengt Lasers," IEEE J.Select.Topics Quantum Electron., vol.3,no.4,pp.1058-64,1997.

10- J.U.Kang,R.Sova,C.Kim, "Tunable multi-wavelength fiber lasers and their applications Proc.SPIE,vol.4645,pp.1-7,2002.

11- A.Yariv "Optical Electronics in modern communications" page 24,2000.

12- X.Shu,S.Jiang,D.Huang, "Fiber grating Sagnac loop and its multiwavelength laser application," IEEE Photon.Technol.Lett.,vol.12, no.8,pp. 980-983, 2000.

13- C.S. Kim, Y.G.Han, R.M.Sova, U.C.Paek,Y.Chung, J.U.Kang "Optical fiber modal birefringence measurement based on Lyot-Sagnac interferometer," IEEE Photon. Technol. Lett.,vol. 15,no.2, pp.269-271,2003.

14- X.Fang,R.O.Claus ,"Polarization-independent all fiber wavelength –division multiplexer based on a Sagnac interferometer," Opt.Lett.,vol.20,no.20,pp.2146-48,1995.

15- I.D.Miller,D. B. Mortimore, P. Urquhart, B.J.Ainslie, S.P.Craig,C.A.Millar,D.B.Payne "A Nd^{+3} – doped CW fiber laser using all-fiber reflectors,"Appl.Opt.,vol.26,no.11,pp.2197- 2201,1987.

16- T.A.Birks and P.Morkel "Jones calculus analysis of single-mode fiber Sagnac Reflector, "Appl. Opt.,vol.27,no.15, pp.3107-3113,1988.

17- Y.G.Han,G.Kim,J.H.Lee,S.B.Lee,"Wavelength spacing tunable multi wavelength fiber laser with lasing wavelength selectivity," Opt.Commun.256,pp.98-102,2005.

18- Y.G. Han, G.Kim, J.H.Lee, S.H.Kim, S.Bae Lee, "Lasing Wavelength and spacing switchable multi wavelength fiber laser from 1510 to 620 nm," IEEE Phot. Technol. Lett , vol .17 ,no.5, pp. 989-991, 2005.

19- G. Das, Z. Medendorp and J. Valiunas, " Multiwavelength fiber laser ", CAP congress, Brock University, Canada, 11-14th June, 2006.

Chapter 3

Single-mode high power multiwavelength fiber ring laser using a saturable absorber

3.1 Introduction

A single-mode high power multiwavelength fiber laser has attracted much attention due to its applications in sensor, wavelength division multiplexed optical communication and spectroscopy. An erbium doped fiber has been used as gain medium to produce multiwavelength fiber laser. At room temperature an erbium doped fiber shows homogenous gain broadening. So, it is difficult to produce a multiwavelength laser due to severe mode competition between adjacent lasing wavelengths. Several techniques have been proposed and demonstrated to produce a multiwavelength fiber laser at room temperature by using, a fiber bragg grating [1,2],photonic crystal fiber [3,4,5,6], dispersion-shifted fiber [7] etc. In most of the cases the application of these lasers are limited due to low output power, large linewidth etc. A few high power multiwavelength fiber laser are reported where an $Er^{+3} - Yb^{+3}$ co-doped fiber is used as a gain medium [8,9]. In chapter 2, we mentioned a multiwavelength fiber laser using bidirectional

pumping scheme in Fabry-Perot resonator configuration. But the output power of the laser is very small ($\approx 3mW$). In this chapter, we demonstrate a high power multiwavelength fiber laser in ring resonator configuration. An $Er^{+3} - Yb^{+3}$ co-doped double clad fiber is used as a gain medium. A Sagnac loop filter is used inside the ring cavity to obtain the desired separation between lasing lines. An unpumped polarization maintaining fiber is used as the saturable absorber to produce stable single mode lasing lines.

3.2 Saturable absorber

A stable single-mode laser with narrow line width is attractive for its application. One of the techniques to get such lasing lines is using the self-induced grating which can dynamically adjust itself to small ambient disturbances. A saturable absorber (SA) is a photosensitive fiber which can be made by doping some impurity like Erbium in glass. Using counter propagating waves in saturable absorber we can make a dynamic grating filters with line width of few hundred hertz. In Figure 3.1, E_1 and E_2 are electric fields of counter propagating waves which are forming standing wave pattern in the saturable absorber. Considering their interference we can write the optical intensity distribution as [10],

$$I = I_1 + I_2 + 2\sqrt{I_1 I_2}\cos(2\beta z) \tag{3.1}$$

where $I_{1,2}$ is the optical intensity of the $E_{1,2}$, z is the propagation distance and β is the propagation constant. The standing wave pattern in SA produces spatial hole burning

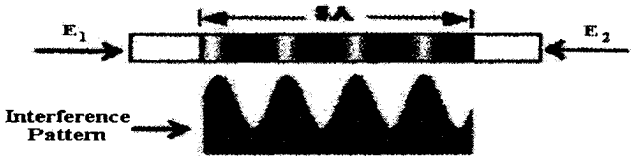

Figure 3.1 Spatial interference in saturable absorber by two counter propagating waves

effect. So in the region of high (anti-nodes) and low (nodes) intensities, the absorption would be low and high respectively. This will create a periodic variation of refractive index with a spatial period of one half of propagating wavelength in saturable absorber. The modulated refractive index which will form a transient grating can be expressed as [11,12,13],

$$n(z) = n_{\circ} + \Delta n \cos(2\beta z) \tag{3.2}$$

where $n_{\circ}$ is the average refractive index change and Δn is the amplitude of induced refractive index perturbation. Δn is typically within $10^{-7} - 10^{-2}$ and based on theoretical study the maximum induced refractive index change in an erbium doped fiber is given by [14,15],

$$\Delta n_{\max} = \frac{\Gamma N \lambda \sigma}{4\pi} \tag{3.3}$$

where Γ is the overlap factor; N is erbium concentration; σ is erbium emission cross section and λ is the wavelength. Equation 3.3 explicitly gives us the relation between induced refractive index change and erbium ion concentration in saturable absorber.

The transient grating formed inside the SA is related to material excitation, so lifetime of excitation dictates the time scale on which the grating is established or decayed. When the two counter propagating beams in SA have different frequencies,

(f_1 and f_2), we observe different interference pattern [16]. Comparing the frequency difference with response time of active-ion, τ (for erbium-ion $\tau \approx 10 m\sec$) , when $|f_1 - f_2| < \frac{1}{\tau}$ or $f_1 = f_2$ we can see an interference pattern in SA which results in spatial hole burning(SHB). When $|f_1 - f_2| > \frac{1}{\tau}$, the saturation can not follow the modulation coming from the interference of the two waves, so no SHB is formed and the saturation is spatially uniform as shown in Figure 3.2 [17].

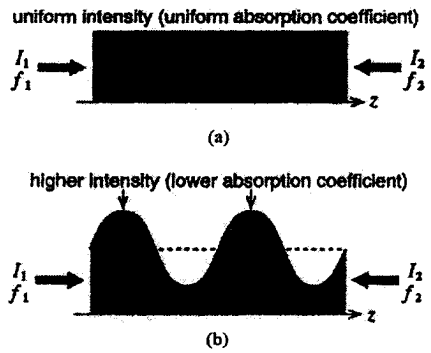

Figure 3.2 Frequency dependent intensity distribution in the SA (a) without SHB, $|f_1 - f_2| >> \frac{1}{\tau}$ (b) with SHB, $|f_1 - f_2| < \frac{1}{\tau}$

So, when the coherency between two counter propagating waves in SA reduces, the reflection of induced grating formed in SA decreases. Furthermore, when the intensity of counter propagating waves inside the SA increases and comes close to saturation point the absorption of SA decreases and medium becomes transparent (Figure 3.3).

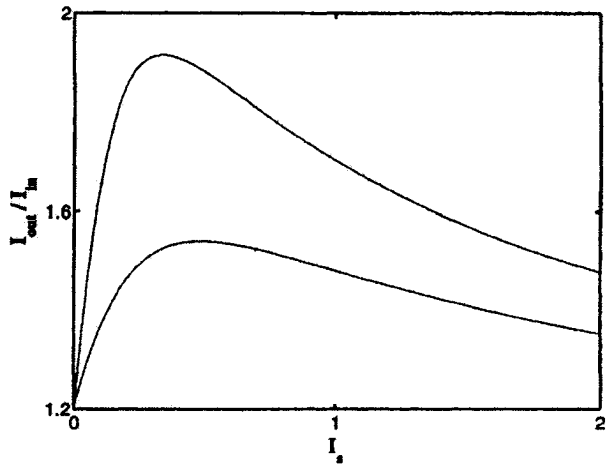

Figure 3.3 Reflectivity of dynamic grating versus the normalized signal intensity for the case when two counter-propagating signals are coherent(upper most curve) and for the case when the signal waves are not coherent[18]

3.3 Saturable absorber grating response

Using coupled mode theory we can find the characteristics of dynamic fiber grating. The coupled differential equations for the counter-propagating signal waves in SA section are [19,20,21],

$$\frac{dA_1}{dz} = \tilde{g}A_1 - kA_2 \exp(2i\Delta K' z) \tag{3.4}$$

$$\frac{dA_2}{dz} = -\tilde{g}A_2 + kA_1 \exp(-2i\Delta K' z)$$

where

$E_{1,2} = A_{1,2} \exp(i(\pm K_{1,2} - \omega_{1,2}t))$ are the field of two counter propagating waves,
A_1 and A_2 are amplitudes of the counter propagating waves E_1 and E_2

$k = \dfrac{g\langle A_1 A_2^* \rangle}{I_S}$ is the coupling term

$$\tilde{g} = g\left(1 - \frac{\langle I_1 + I_2 \rangle}{I_S}\right)$$

$$I_{1,2} = |A_{1,2}|^2$$

$\chi = \frac{\chi_0}{1 + \frac{I}{I_s}}$ is the nonlinear susceptibility

$g = \frac{k_{\chi_0}}{2}$ and I_S represents the effect of saturation

The first term in Equation 3.4 arises from the saturation induced by counter-propagating waves. The second term which gives the reflection from grating arises from the grating formed by the interference of two waves. Using the boundary conditions of $A_1(0) = 1$ and $A_2(L) = 0$, where L is the length of dynamic grating, we can obtain solutions of Equation 3.4 which gives the response of the dynamic grating as

$$A_1(z) = \frac{S\,Cosh[S(L-z)] + (i\Delta K' - \tilde{g})Sinh[S(L-z)]}{S\,Cosh(SL) + (i\Delta K' - \tilde{g})Sinh(SL)} \exp(i\Delta K' z)$$

$$A_2(z) = k\frac{Sinh[S(z-L)]}{S\,Cosh(SL) + (i\Delta K' - \tilde{g})Sinh(SL)} \exp(-i\Delta K' z) \tag{3.5}$$

where $S = \sqrt{(\tilde{g} - i\Delta K')^2 - k^2}$. From Equations 3.5, the reflection as a function of wavelength and grating length can be expressed as,

$$R(\lambda, L) = \left|\frac{A_2(0)}{A_1(0)}\right|^2 = k^2 \frac{Sinh^2(SL)}{[S\,Cosh(SL) + (i\Delta K' - \tilde{g})Sinh(SL)]^2} \tag{3.6}$$

Equation 3.6 can be used to plot the reflection as a function of grating length for different values of refractive index change(k) [22]. The reflection bandwidth of the dynamic grating is given by

$$\Delta\nu = \frac{c}{2\pi\, n}\sqrt{\left(\frac{\pi}{L}\right)^2 + \frac{|k|^2}{1+\left(\tilde{g}L/\pi\right)^2}} \tag{3.7}$$

where n is the refractive index. So the bandwidth of dynamic grating depends on the length of SA and strength is a function of active-ion concentration [23].

3.4 Experimental set up, results and discussion

Figure 3.4 shows a ring resonator configuration to produce high power multiwavelength fiber laser. The ring cavity comprises a piece of double clad $Er^{+3}-Yb^{+3}$ co-doped fiber which serves as the gain medium of the laser. The active fiber is pumped by a 975 nm laser diode with maximum output power of 4 w at 4 A current, through a 6×1 pump power combiner (Appendix III). A saganc loop filter (chapter 2, section 3.2) is employed to generate a spectrum at a particular wavelength spacing. An optical isolator (OI) is used inside the cavity to confirm unidirectional propagation of light. A polarization controller (PC1) is used to control the state of polarization of the circulating wave inside the cavity. The output of the laser is extracted by a 3 dB coupler. An optical spectrum analyzer (OSA) with resolution of 0.05 nm is used to do the measurements.

A single mode circular core double clad $Er^{+3}-Yb^{+3}$ co-doped fiber (SM-EYDCF) and a single-mode polarization-maintaining double clad $Er^{+3}-Yb^{+3}$ co-doped fiber (PM-EYDCF) are used as the gain media. The splice loss at single-mode

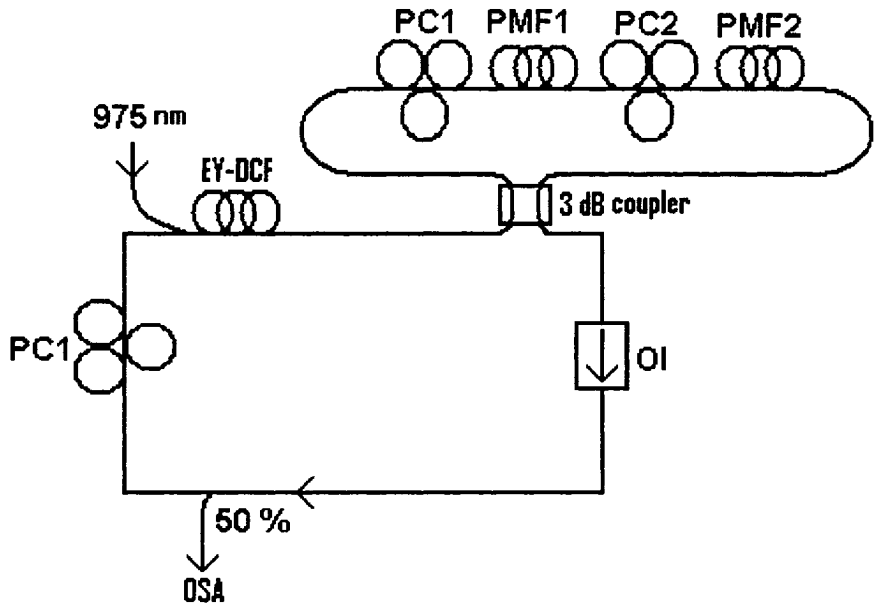

Figure 3.4 schematic of the set up for multi-wavelength fiber laser

and active fiber is less than 1 dB. PM-EYDCF has a hexagonal shape of cross section for second cladding in order to increase the pump absorption efficiency through multiple reflection from outer surface. The data for both SM-EYDCF (Nufern: SM-EYDF-7/130) and PM-EYDCF (CorActive: HPA-EY-10-PM-01) are mentioned in Table 3.1(a,b). Figure 3.5 shows variation of pump wavelength with pump current. Figure 3.6(a) and 3.6(b) show the absorption spectrum of PM-EYDCF and SM-EYDCF with the peak absorption of $\approx$ 9.3 dB/m and 2 dB/m at wavelength of $\approx$ 975 nm respectively.

CorActive: HPA-EY-10-PM-01	
Parameters	**Value**
Pump guideYtterbium absorption @ 975 nm	$9.3\,dB/m$
Core absorption (Er/Yb)@ 1550 nm	$21\,dB/m$
Effective numerical aperture	0.17
Cladding numerical aperture	0.47
Birefringence	0.000169
Core diameter	$9.8\,\mu m$
Length	1.7 m

(a)

Nufern: SM-EYDF-7/130	
Parameters	**Value**
Pump guideYtterbium absorption @ 975 nm	$2\,dB/m$
Peak core Erbium absorption near 1550 nm	15 dB/m
Core numerical aperture	0.17
Cladding numerical aperture	0.46
Second mode cut off	1450 ± 50 nm
Clad diameter	$130 \pm 3\,\mu m$
Length	4.5 m

(b)

Table 3.1 (a) and (b) Gain medium fiber data

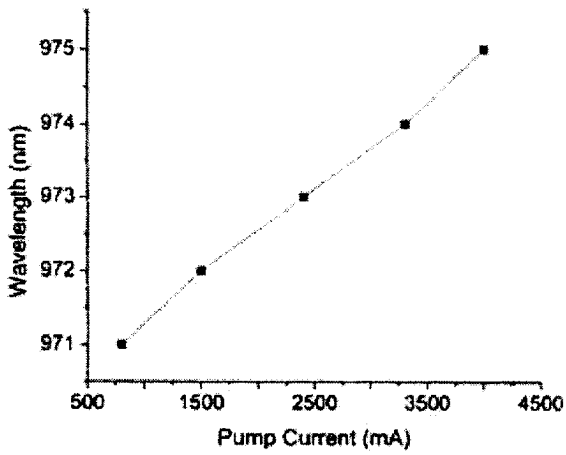

Figure 3.5 Current-wavelength characteristic of pump source

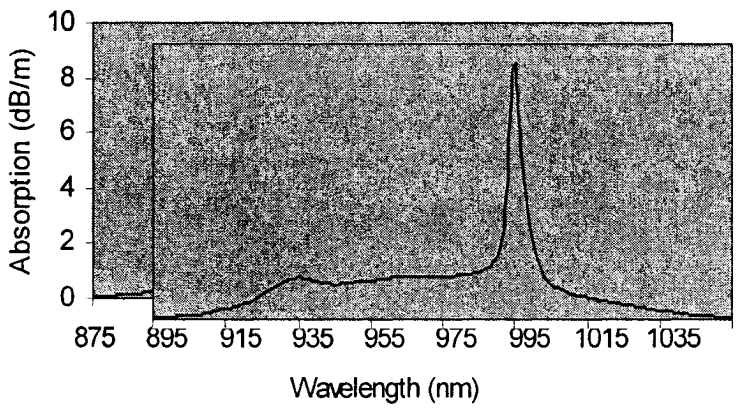

(a)

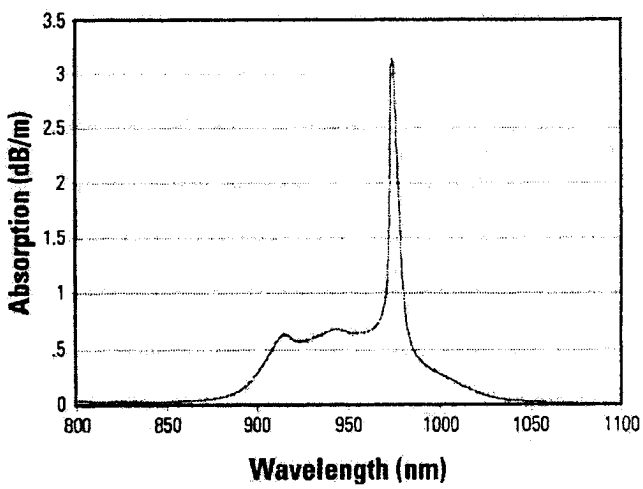

(b)

Figure 3.6 (a) Absorption spectrum of PM-EYDCF2 (b) Absorption spectrum of SM-EYDCF

To study the tunability of the spacing in real time using multi – segment Sagnac loop (chapter 2, Equation 2.13) in ring resonator, we provided a two segment Sagnac loop with PMF lengths of $L_1 = 2m, L_2 = 4m$, which produces a separation of 1.1 nm and 3.4 nm. For each gain medium at particular lasing line separation we tried to find out the spectra showing the maximum number of lasing lines with maximum output power. Figure 3.7 shows output of multiwavelength laser with a maximum output power of 176 mW using SM-EYDCF. We can Switch from $\Delta\lambda \approx 1.1nm$ to $\Delta\lambda \approx 3.4nm$ by adjusting PCs in Sagnac loop filter. Figure 3.8 shows maximum number of lasing lines with maximum output power of 174 mW using SM-EYDCF .

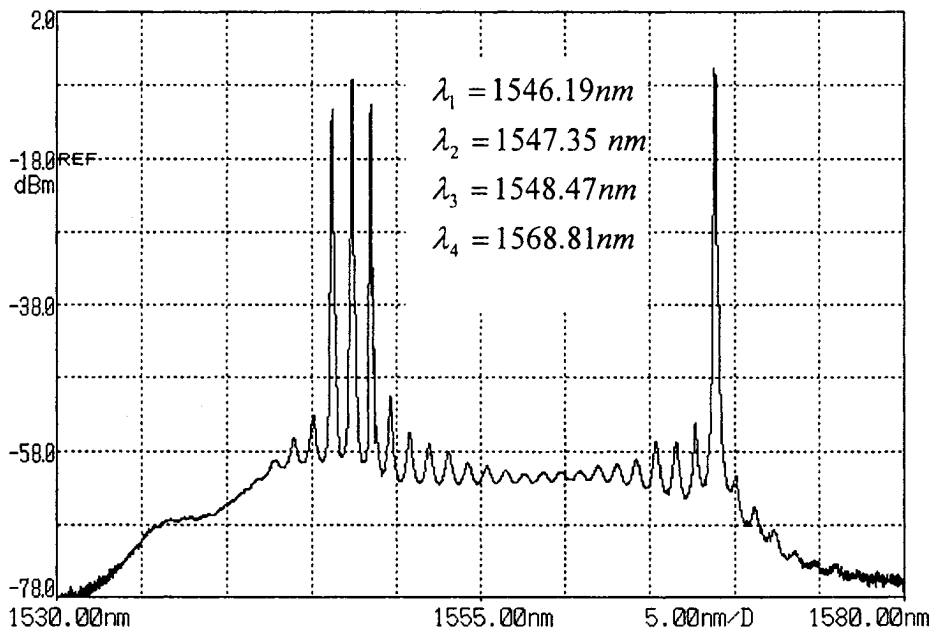

Figure 3.7 Spectrum of four lasing lines, $\Delta\lambda \approx 1.1nm$, $L_B = \frac{\lambda}{B} = 4\ mm$, resolution=0.05 nm, $P_{in} = 1873$ mW, $P_{out} = 176$ mW, Stability $\leq$ 10 min

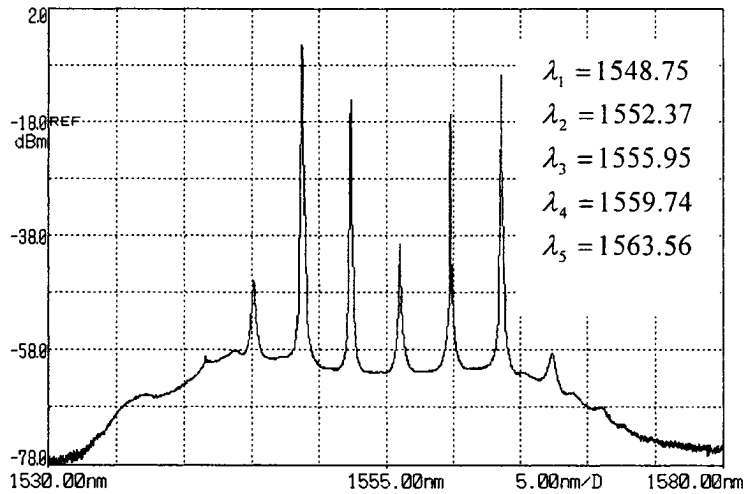

Figure 3.8 Spectrum of five lasing lines, $\Delta\lambda \approx 3.4\,nm$, $L_B = \frac{\lambda}{B} = 4\ mm$, resolution=0.05 nm, $P_{in} = 1873$ mW , $P_{out} = 174$ mW, Stability $\approx$ 2-3 successive scans

We repeated the experiment using PM-EYDCF as the gain medium. Figure 3.9 and Figure 3.10 show the multiwavelength lasing lines with maximum output power of 86 and 98 mW at $\Delta\lambda \approx 1.1\,nm$ and $\Delta\lambda \approx 3.4\,nm$ respectively.

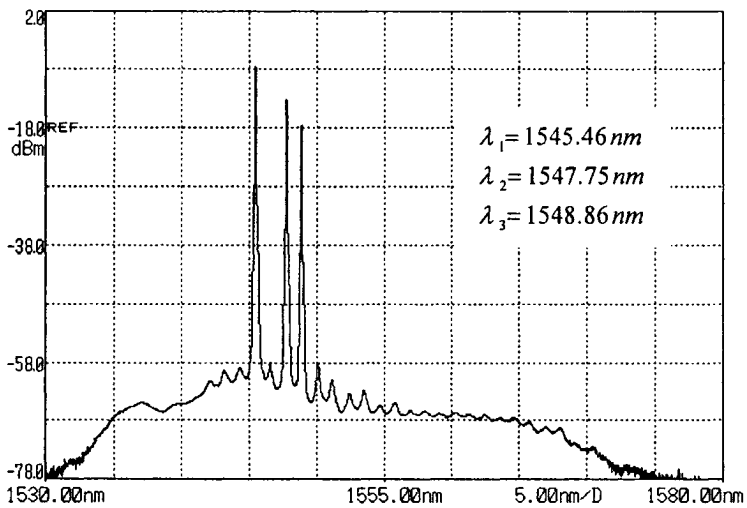

Figure 3.9 Spectrum of 3 lasing lines, $\Delta\lambda \approx 1.1\,nm$, $L_B = \frac{\lambda}{B} = 4\ mm$, resolution=0.05 nm, $P_{in} = 1160$ mW , $P_{out} = 86$ mW, Stability $\approx$ 2 successive scans

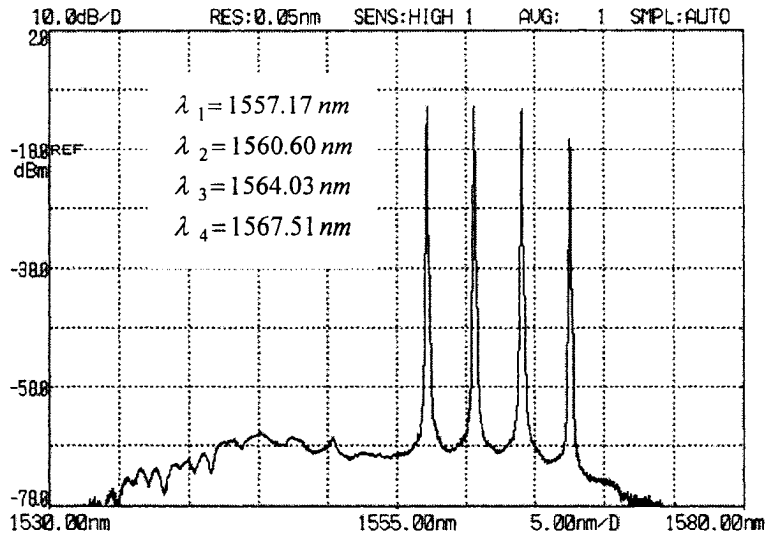

Figure 3.10 Spectrum of four lasing lines, $\Delta\lambda \approx 3.4\,nm$, $L_B = \frac{\lambda}{B} = 4\ mm$, resolution=0.05 nm, $P_{in} = 1516$ mW, $P_{out} = 98$ mW, Stability $\approx$ 2-3 successive scans

Though we can produce multiwavelength laser with more than 100 mW output power, they are not stable and severe mode hopping exists. In order to stabilize them we modified the resonator in Figure 3.4 by incorporating SA section in circuit.

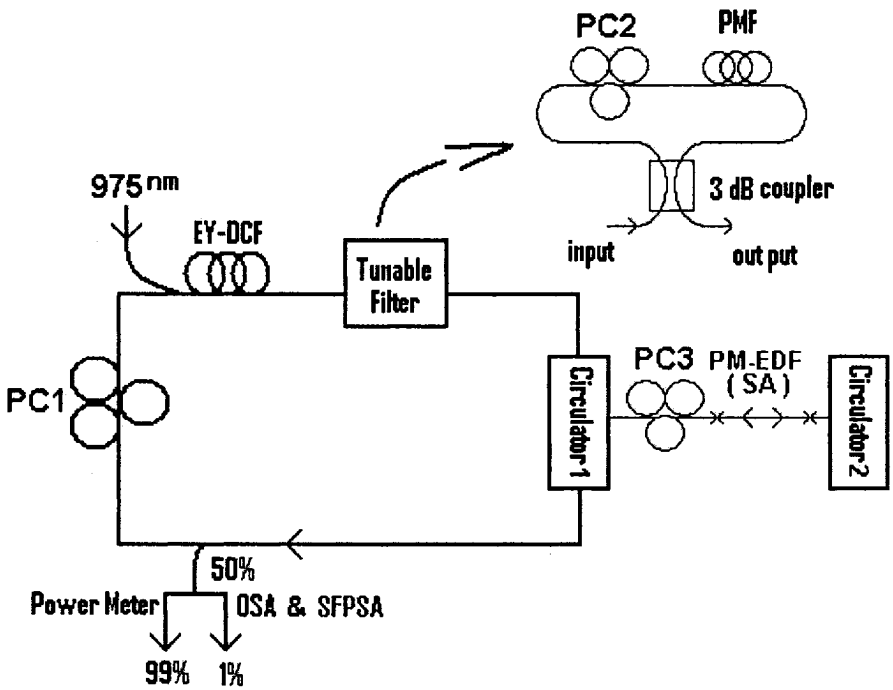

Figure 3.11 Schematic of the set up for stable multi-wavelength fiber laser

Figure 3.11 shows the ring resonator for producing multiwavelength fiber laser using SA. An unpumped elliptical core erbium doped fiber is used inside the cavity as SA, a polarization controller (PC3) to maintain the polarization of the wave inside the SA, two polarization independent optical circulator, circulator1 ensures unidirectional propagation of the wave inside the cavity and the optical circulator2 acts as a broadband reflector (ports 2 and 3 are spliced) (Figure 3.12). The reflected light interferes with counter propagating wave and creates standing wave pattern inside the SA section.

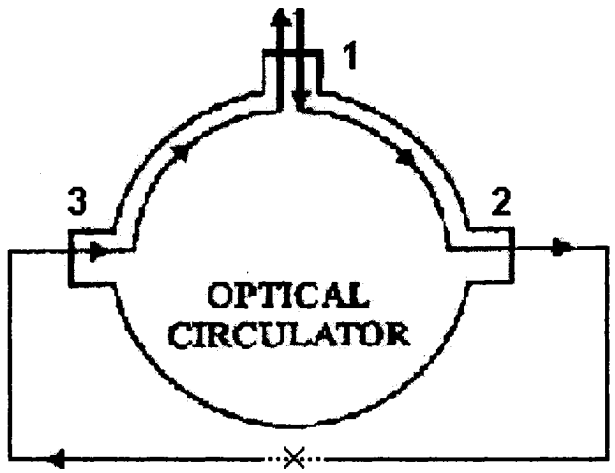

Figure 3.12 Optical circulator as reflector .ports 2 and 3 are connected

The output power is extracted through a 3 dB coupler. An optical spectrum analyzer (OSA) with the resolution of 0.05 nm and a scanning Fabry-Perot spectrum analyzer (SFPSA) of resolution 27 MHz (FSR=8 GHz, Finesse=300) are used to monitor the output of the laser. The high resolution of SFPSA helps us to study the longitudinal-mode characteristic of each lasing line.

The combination of fibers we used as gain and SA are listed in Table 3.2. As mentioned in Table 3.2 two types of elliptical core erbium-doped fiber (PM-EDF1 or PM-EDF2) with different erbium concentration and length is used as the SA inside the cavity. Figures 3.13 and 3.14 show the absorption spectrum of PM-EDF1 and PM-EDF2. The peak absorption of PM-EDF1 and PM-EDF2 for signal ($\lambda = 1550$ nm) is 10.8 dB/m and 19 dB/m respectively.

<table>
<tr><th>Gain Medium Fiber</th><th>Saturable Absorber Fiber</th></tr>
<tr><td rowspan="2">Single Mode Erbium-Ytterbium Doped Double Clad Fiber (SM-EYDCF)</td><td>Polarization Maintaining Erbium Doped Fiber (PM-EDF1)</td></tr>
<tr><td>IVG : Polarization Maintaining Erbium Doped Fiber (PM-EDF2)</td></tr>
<tr><td rowspan="2">Polarization Maintaining Erbium-Ytterbium Doped Double Clad Fiber (PM-EYDCF)</td><td>Polarization Maintaining Erbium Doped Fiber (PM-EDF1)</td></tr>
<tr><td>IVG : Polarization Maintaining Erbium Doped Fiber (PM-EDF2)</td></tr>
</table>

Table 3.2. Different types of fiber used in the experiments

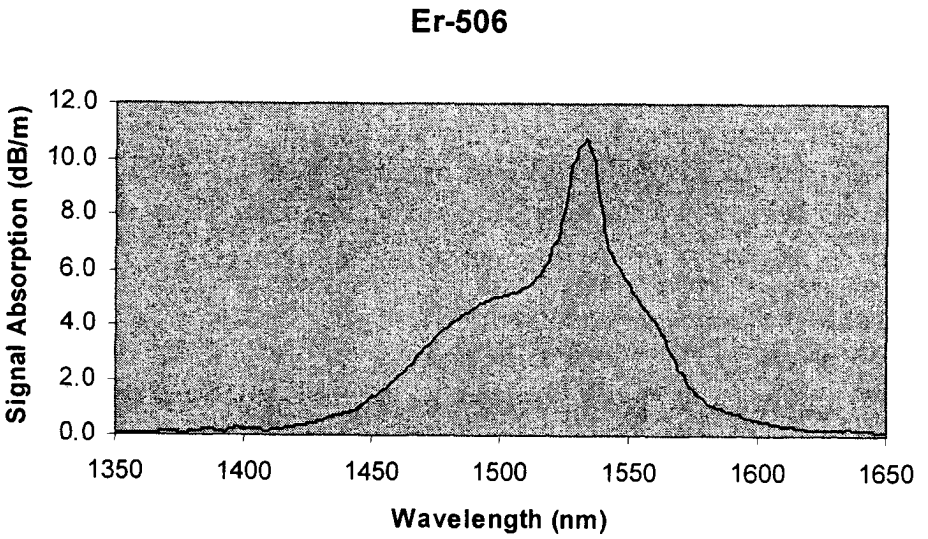

Figure 3.13 Absorption spectrum of PM-EDF1

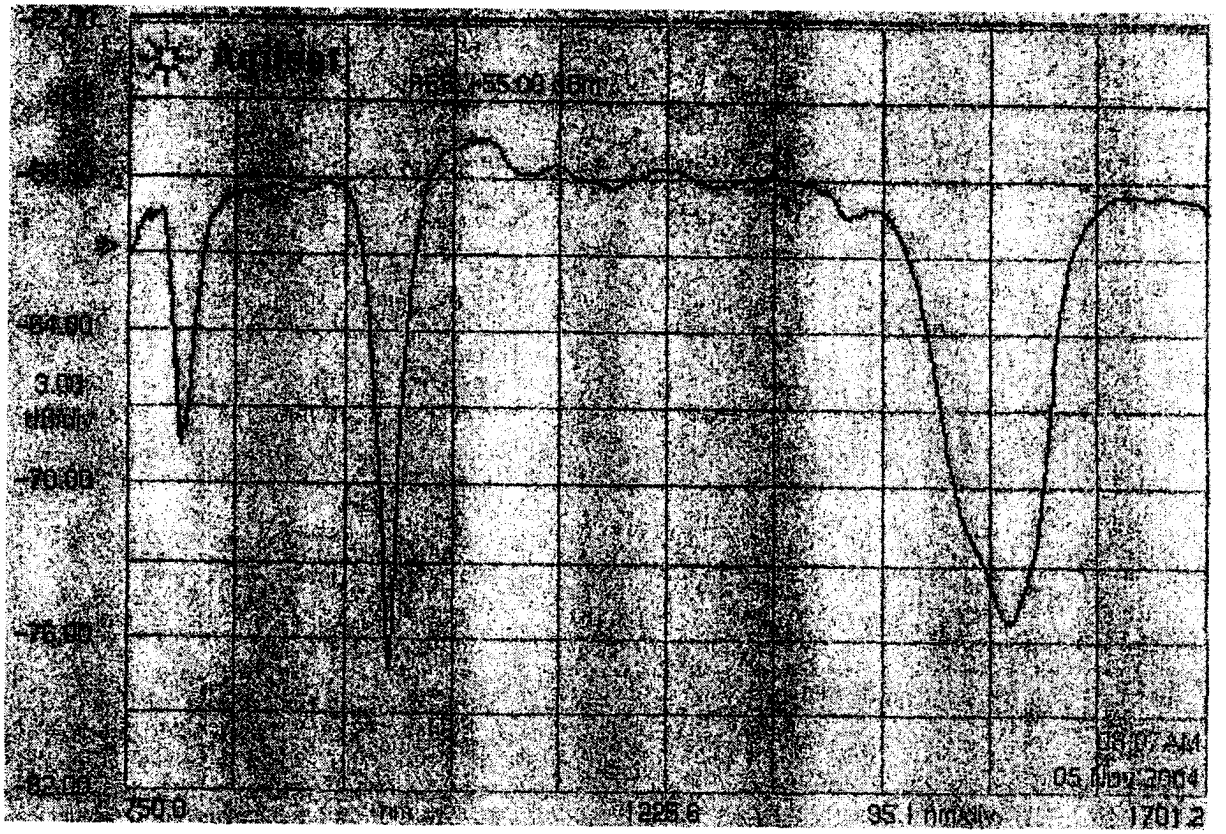

Figure 3.14 Absorption spectrum of PM-EDF2

Our experimental observation shows that using SA in circuit we can improve the stability of lasing lines. Figure 3.15 shows 4-lasing lines using PM-EYDCF as the gain medium and without using SA. The lasing lines are stable only for few minutes. Figure 3.16 shows 4 lasing lines using 3 m of PM-EDF1 inside the resonator (Figure 3.11). The lasing lines are stable for more than 2 hours when measured using OSA of resolution 0.01 nm. To study the effect of separation on stability we changed the separation between lines from 1.5 to 0.8 nm by changing the length of polarization-maintaining fiber inside the Sagnac loop filter. Figure 3.17 shows 4 stable lasing lines of separation 0.8 nm when observed through an OSA of resolution 0.05 nm. Analyzing the output using a Scanning Fabry-Perot Spectrum Analyzer (SFPSA) we found that the lasing lines are single-mode but suffering from severe mode hopping.

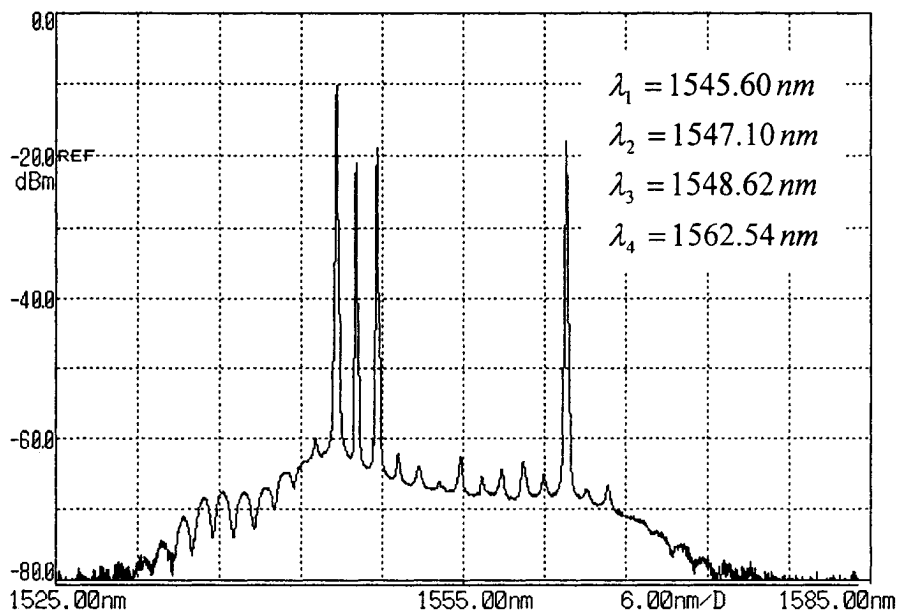

Figure 3.15 4-lasing lines with stability of few minutes at resolution of 0.05 nm through OSA. PM-EYDCF is used as gain medium and without using SA. P_{in} = 1160 mW , P_{out} = 98 mW. $\Delta\lambda = 1.5\,nm$;Length of PMF is $\approx 4m$,Birefringence = 3.78×10^{-4}

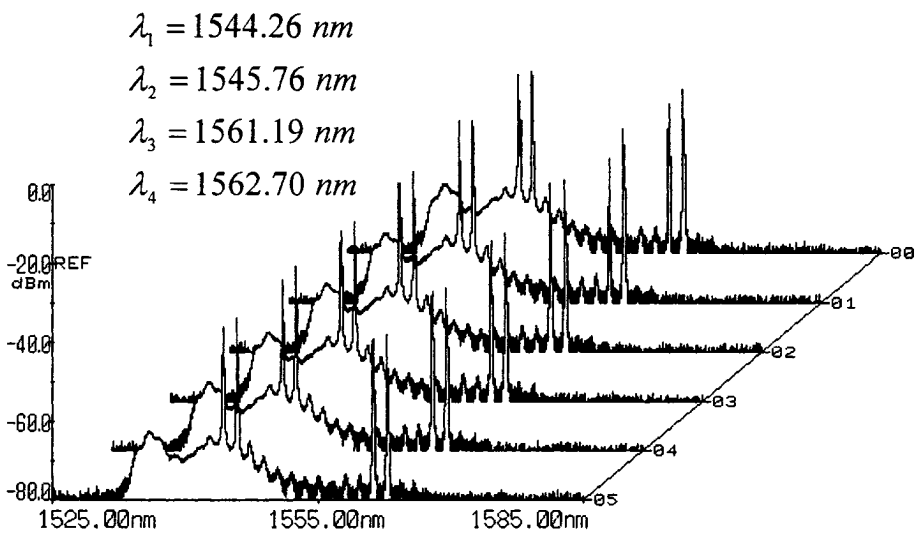

Figure 3.16 Stability of 4 lasing lines over 2 hours at resolution of 0.01 nm using PM-EYDCF and 3 m of PM-EDF1 as SA obtained through OSA. P_{in} = 1160 mW , P_{out} = 66 mW. $\Delta\lambda = 1.6\,nm$;Length of PMF is $\approx 4m$,Birefringence = 3.78×10^{-4}

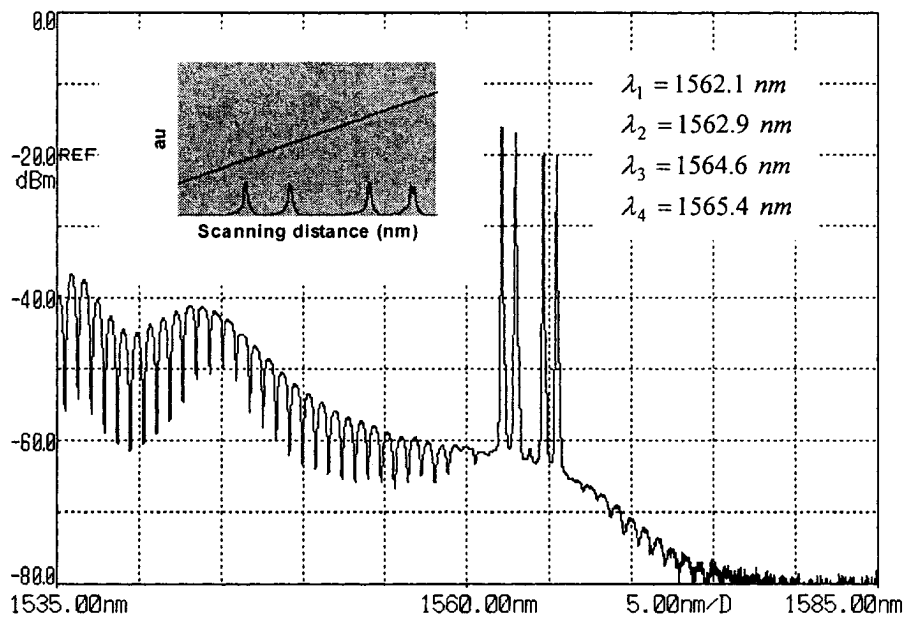

Figure 3.17 Stability of 4 lasing lines at resolution of 0.05 nm using PM-EYDCF and 3 m of PM- EDF1 as SA. $P_{in} = 947mW$, $P_{out} = 50\ mW$. Inset shows spectrum plotted using data extracted from SFPSA. $\Delta\lambda = 0.8\,nm$; Length of PMF is $\approx 8m$,Birefringence = 3.78×10^{-4}

To study the effect of SA we used two types of PM-EDF as SA with different concentration of active-ion and lengths. We performed our experiments using several lengths of PM-EDF2 (from 15 cm-3 m) as SA. The best result is obtained using 15 cm of PM-EDF2 as SA and SM-EYDCF as gain medium. We can produce two stable lines with stability of more than 2 hours at resolution of 0.01 nm (Figure 3. 18).

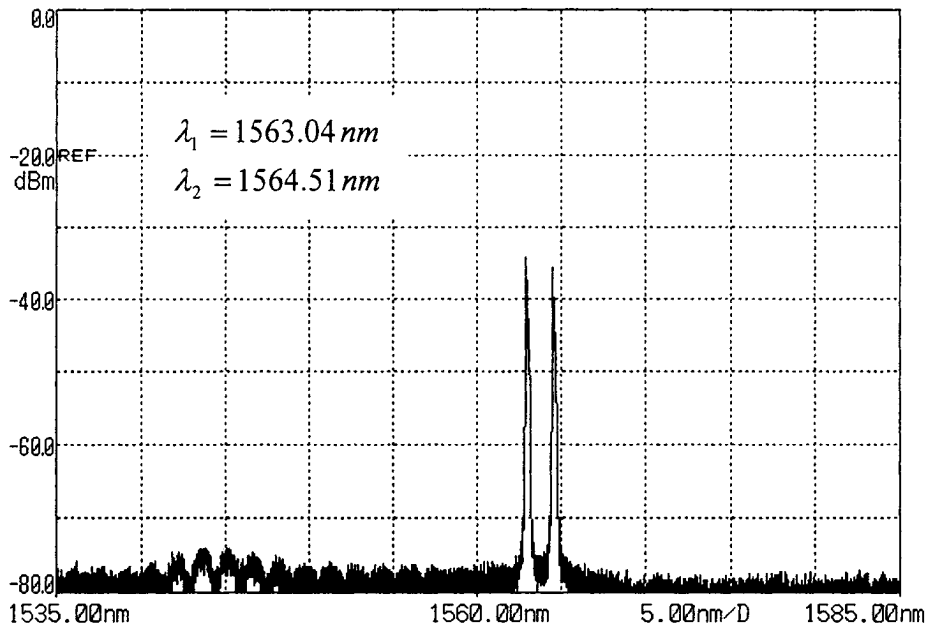

Figure 3.18 Stability of 2 lasing lines at resolution of 0.01 nm using PM-EYDCF and 15 cm of PM- EDF2 as SA.

$P_{in} = 947\,mW$. $P_{out} = 42\ mW$, $\Delta\lambda = 1.6\ nm$; Length of PMF is $\approx 4m$,Birefringence $= 3.78 \times 10^{-4}$

We repeated the experiment using PM-EDF1. Our experiments show that PM-EDF1 gives us better stability of lasing lines with high output power when length varied from 1 to 3 m, because it has low absorption compared to PM-EDF2 (Figure 3.13,3.14).

We repeated the experiment using SM-EYDCF as the gain medium and PM-EDF1 as the SA. We could produce a maximum of four stable lasing lines when observed through OSA of resolution 0.01 nm with stability of more than 2 hours. The stability of the lasing lines depends on the stability of the dynamic grating inside the SA. A good

polarization-maintaining is required to produce a stable grating. Comparing results using SM-EYDCF and PM-EYDCF as gain medium we can conclude that the PM-EYDCF maintained the state of polarization inside the cavity and resulted in more stable lasing lines. Figure 3.19(a) and 3.19(b) show a stable single-mode dual wavelength laser with an output power of 50 mW for an input pump power of 947 mW. The laser produces a maximum output power of 110 mW for two stable lasing lines with stability more than 2 hours for an input pump power of 1873 mW when observed through OSA. Figure 3.20(a), 3.20(b) show a highly stable single- mode lasing line with the output power of 50 mW for an input pump power of 947 mW. Figure 3.21 shows the output intensity variation ($\leq$ 0.15 dB) of single-mode single wavelength laser.

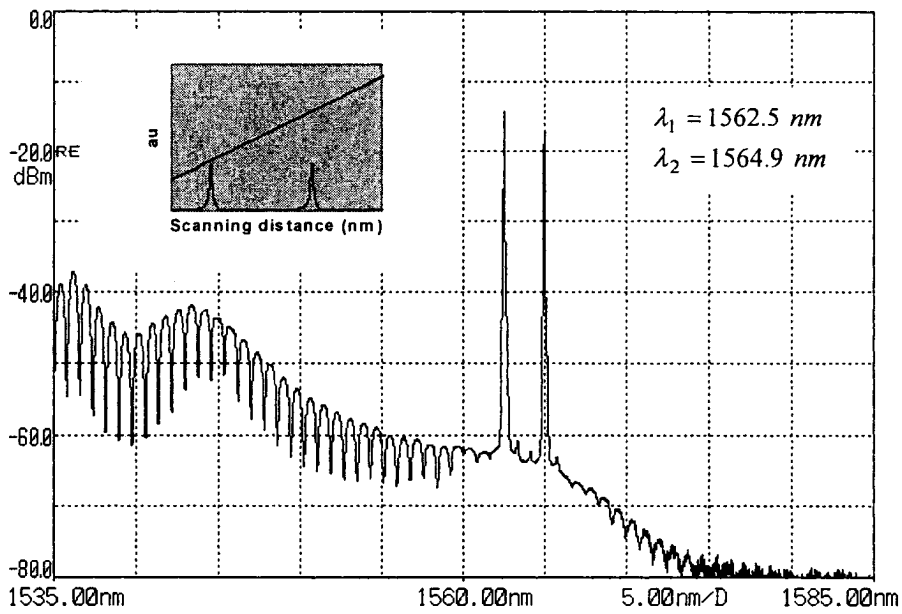

(a)

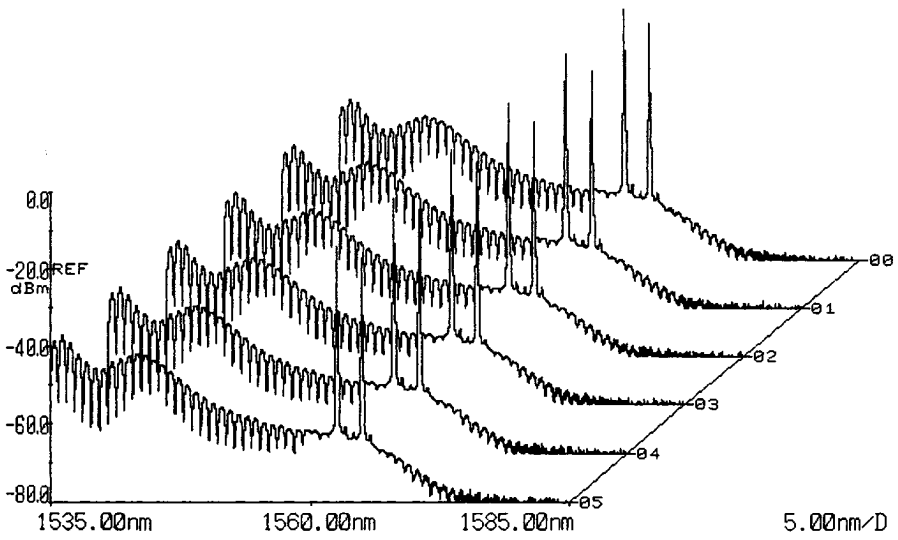

(b)

Figure 3.19 (a) 2 stable lasing lines at resolution of 0.05 nm using PM-EYDCF and 3 m of PM- EDF1 as SA. $P_{in} = 947\ mW$, $P_{out} = 50\ mW$. Inset shows two stable single mode lasing lines plotted using data extracted from SFPSA. Length of PMF is $\approx 8m$,Birefringence $= 3.78 \times 10^{-4}$ (b) stability of 2 single-mode lasing lines for multiple scans over 2 hours.

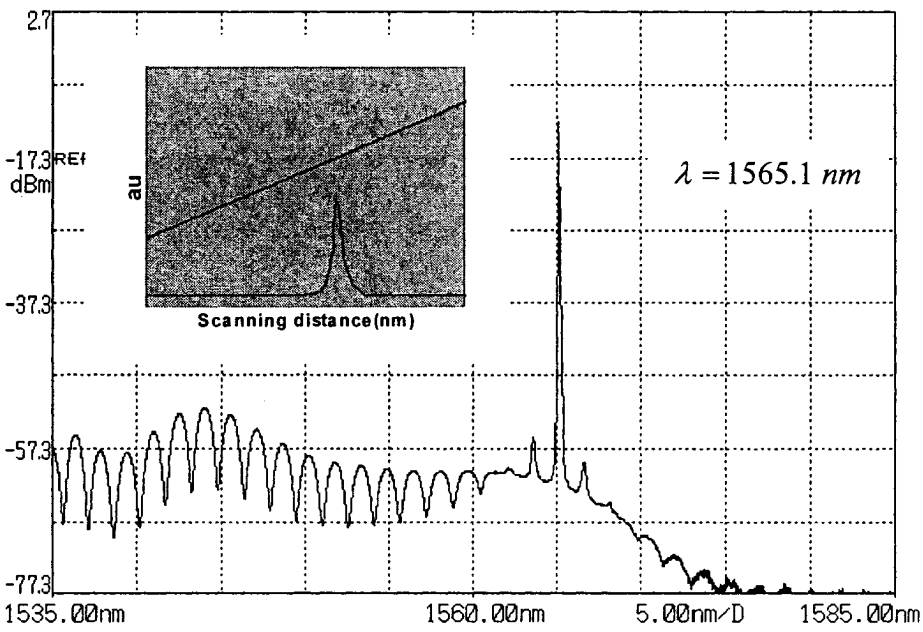

(a)

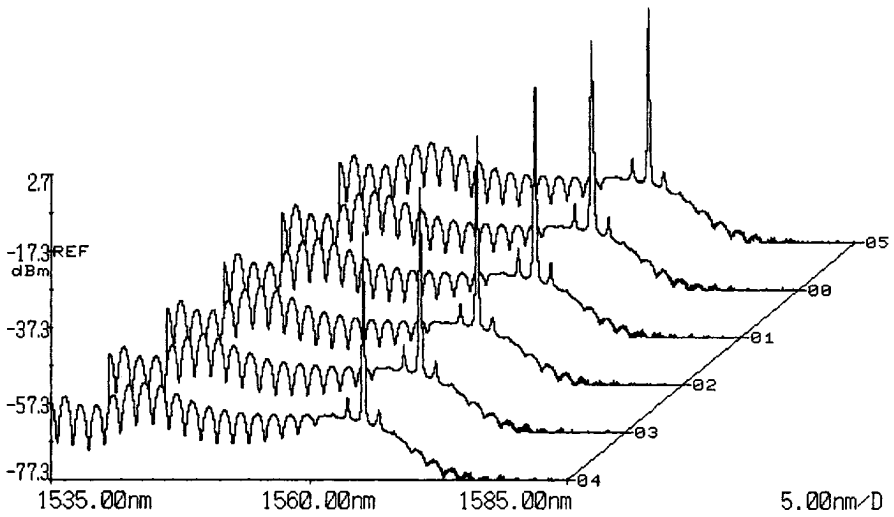

(b)

Figure 3.20 (a) Highly stable single lasing line at resolution of 0.05 nm using PM-EYDCF and 3 m of PM- EDF1 as SA. $P_{in} = 947mW$, $P_{out} = 50\ mW$. Inset shows one highly stable single mode lasing line plotted using data extracted from SFPSA (b) stability of one single mode lasing line for multiple scans over 2 hours.

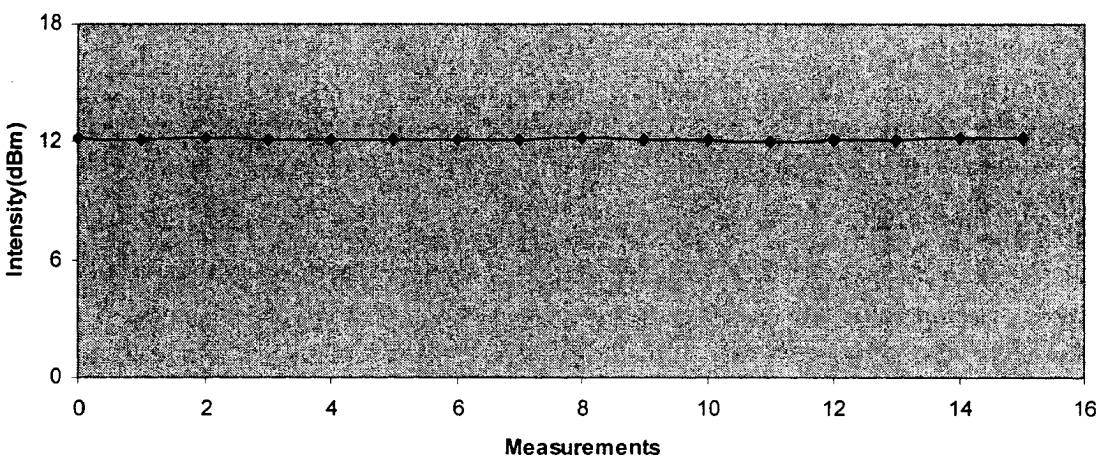

Figure 3.21 Intensity fluctuation for single stable lasing line

In our study the minimum and maximum separation between two adjacent lasing lines for stable multiwavelength operation are 0.8 and 3.2 nm respectively. As mentioned earlier (chapter 2), the spectrum modulation bandwidth by Sagnac loop filter is inversely proportional to the polarization-maintaining fiber (PMF) length in Sagnac loop filter. By increasing the PMF length we decrease the modulation bandwidth which makes fewer adjacent longitudinal modes oscillate. So, with fewer adjacent modes we have more chance to get lasing lines with less mode hopping. PCs adjustments in circuit have the crucial role in obtaining stable lasing lines. Using polarization-maintaining $Er^{+3} - Yb^{+3}$ co-doped fiber as gain medium and adjusting PCs we can produce quasi-linearly polarized light inside the cavity which gives us better stability of the transient grating. By proper adjustment of the cavity PC, it is possible to produce a linearly polarized single wavelength laser.

In order to find the highest number of stable lasing lines we have to optimize the length of SA; concentration of active-ion in SA; and the signal light power that writes the dynamic grating in SA. Theoretically, considering a SA, doped with a particular concentration of active-ions and adjusted at particular launch signal power, we can find the optimum length by plotting the reflection versus grating length in Equation 3.6 [22]. Using the plot, effective length can be found at points with over 90 percent reflection. But experimentally, we should change either the input pump power or SA length. Far below or above the saturation point for particular length of SA, the absorption of SA is low. At particular signal power if we use too long a length of SA all signal is absorbed at SA and the output power decreases. So, we used different lengths of SA, at particular launch pump power, to find the optimum length, or for particular length of SA we adjust

the input pump power that gives the stable lasing lines [24]. We studied with different lengths of SA at different active-ion concentration. Considering the Equation 3.3, higher concentration gives more induced refractive index change and eventually stronger induced grating but on the other hand, high absorption related to high concentration of certain ions which reduce the output power. Considering Equation 3.7, the reflection bandwidth of the dynamic grating is inversely proportional to length of SA. So, in order to decrease the reflection bandwidth we should increase the length of SA.

The separation between two longitudinal cavity modes is very small because of long cavity length. The Sagnac loop filter inside the cavity modulates the output of the ring resonator. The full width at half maximum of the filter is large so it selects many cavity modes. So, the output of the laser is multimode. The presence of narrow band transient grating formed inside the cavity help to produce a single mode lasing line. In our experiment counter propagating multiwavelength lasing line create a narrow-multiband transient grating and thus produce stable single-mode multiwavelength fiber laser.

3.5 Conclusion

A simple configuration to generate high power single-mode multiwavelength fiber laser is proposed. Experimentally we showed, we can stabilize the lasing lines using SA in the circuit. Our laser can produce a maximum 4 lasing lines when observed through OSA at resolution of 0.01 nm. Furthermore, polarization-maintaining gain fiber gives better stability of lasing lines. We could get the best result using PM-EYDCF as gain medium and PM-EDF1 of length 3 m as SA. The concentration and length of the SA

plays an important role to stabilize the lasing lines. We can produce a dual wavelength laser with maximum output power of 60 mW when observed through a SFPSA. The optimum range of input pump power to get stable lasing lines is 804-947 mW.

References :

1- D.Wei,T.Li,Y.Zhao,S.Jian, "Multiwavelength erbium-doped fiber ring lasers with overlap-written fiber bragg gratings,"Opt.Lett.,vol.25,no.16,pp.1150-52,2000.

2- D.S.Moon,U.Paek,Y.Chung, " Multi-wavelength lasing oscillations in an erbium doped fiber laser using few-mode fiber bragg garting," Opt.Exp.,vol.12,np.25,pp.6147-52,2004.

3- X.Yang,X.Dong,S.Zhang,F.Lu,X.Zhou,C.Lu, " Multiwavelength Erbium-doped fiber laser with 0.8 nm spacing using sampled Bragg grating and photonic crystal fiber," IEEE Photon. Technol. Lett., vol.17,no.12,pp.2538-40,2005.

4- A.Zhang,M.S.Demokan,H.Y.Tam, "Room temperature multiwavelength erbium-doped fiber ring laser using a highly nonlinear photonic crystalfiber," Opt.Commun.260,pp.670-4,2006.

5- X.Liu,X.Yang,F.Lu,J.Ng,X.Zhou,Chao Lu, " Stable and uniform dual- wavelength erbium-doped fiber laser based on fiber Bragg gratings and photonic crystal fiber,"Opt. Exp., vol.13, no.1, pp.142-7 ,2005.

6- S.Pan,C.Lou,Y.Gao, "Multiwavelength erbium – doped fiber laser based on inhomogeneous loss mechanism by use of a highly nonlinear fiber and a Fabry-Perot filter," Opt.Exp.,vol.14,no.3 pp.1113-18,2006.

7- A.Zhang,M.S.Demokan,H.Y.Tam, "Room temperature multiwavelength erbium-doped fiber ring laser using a highly nonlinear photonic crystalfiber," Opt.Commun.260,pp.670-4,2006.

8- T. Qiu, L. Li, A. Schulzgen, V. L. Temyanko, T. Luo , S. Jiang, A. Mafi, J. V. Moloney, N.Peyghambarian, "Generation of 9.3 W multimode and 4 W single

mode output from 7 cm short fiber lasers," IEEE Photon. Technol. Lett., vol.16,no.12,pp.1-3,2004.

9- Z.G.Lu,F.G.Sun,G.Z.Xiao,P.Lin,P.Zhao, "High-power multiwavelength Er-Yb codoped double-cladding fiber ring laser," IEEE Photon. Technol. Lett., vol.17,no.9,pp.1821-23,2005.

10- Born and Wolf, "Principles of Optics," 7th (Expanded) edition ,Cambridge, pp.288, 1999.

11- S.J.Frisken, "Transient Bragg reflection grating in erbium-doped fiber amplifiers," Opt. Lett.,vol.17,no.24,1992.

12-Y.O.Barmenkov,A.V.Kiryanov,M.V.Andres, "Dynamic bragg grating induced in erbium-doped fiber at phase-modulated beams'coupling,"IEEE J.Quantum Electron.,vol.41,no.9,pp.1176-1180,2005.

13-M.Horowitz,C.R.Menyuk,S.Keren, "Modeling the saturation induced by broad-band pulses amplified in an erbium-doped fiber amplifier," IEEE Photon. Technol. Lett., vol.11,no.10,pp.1235-37,1999.

14-E.Desurvire , "Study of the complex atomic susceptibility of erbium-doped fiber amplifiers"J. Lightwave Tech.,vol.8,no.10, pp.1517-27, 1990.

15-J.Canning,M.G.Sceats, "Transient gratings in rare-earth-doped phosphosilicate optical fibers through periodic population inversion ,"Electron. Lett.,vol.31,no.7,pp.576-77,1995.

16- J.Liu, J.Yao,Jian Yao, T.H.Yeap, " Single-longitudinal-mode multiwavelength fiber ring laser," IEEE Photon.Lett.,vol.16,no.4,pp.1020-22,2004.

17- N.Kishi,T.Yazaki,"Frequency control of a single-frequency fiber laser by cooperatively induced spatial-hole burning," IEEE Photon.Technol.Lett.,vol.11,no.2,pp.182-84,1999

18- Y.Mitnick,M.Horowitz,Baruch Fischer, "Coupling effects of signal and pump beams in three-level saturable-gain media,"J.Opt.Soc.Am.B,vol.15,no.9,pp.2433-38,1998.

19- B.Fischer,J.L.Zyskind,J.W.Sulhoff,D.J.DiGiovanni, "Nonlinear wave mixing and induced grating in erbium-doped fiber amplifiers,"Opt.Lett.,vol.18,no.24,pp.2108-2110,1993.

20- M.Horowitz,R.Daisy,B.Fischer,J.L.Zyskind,"Linewidth-narrowing mechanism in lasers by nonlinear wave mixing," Opt.Lett.,vol.19,no.18,pp.1406-08,1994.

21- M.Horowitz,R.Daisy,B.Fischer, "Filtering behavior of a self-induced three-mirror cavity formed by intracavity wave mixing in a saturable absorber," Opt.Lett.,vol.21,no.4,pp.299-301,1996.

22- D.K.W.Lam,B.K.Garside, "Characterization of single-mode optical fiber filters"Appl. Opt.,vol.21,no.3,pp.440-45,1981.

23- B.Fischer,J.L.Zyskind,J.W.Sulhoff,D.J.DiGiovanni, " Nonlinear four wave mixing in erbium doped fiber amplifiers,"Electron. Lett.,vol.29,no.21,pp1858-59,1993.

24- Y.Cheng,J.T.Kringlebotn,W.H.Loh,R.I.Laming,D.N.Payne, "Stable single-frequency traveling-wave fiber loop laser with integral saturable-absorber-based tracking narrow-band filter,"Opt.Lett.,vol.20,no.8,pp.875-77,1995.

Chapter 4

Future Work

We can increase the stability and number of lasing lines and output power of the laser by improving our design as outlined below:

- Decreasing the whole cavity length to increase the separation between the cavity longitudinal modes. So, we would be able to increase the number of lasing lines which are single mode at resolution of 27 MHz.
- Instead of using circulator as reflector, we can use arrays of bragg gratings to select the particular wavelengths to oscillate in cavity.
- Employing highly doped active fiber as gain medium to get high output power at shorter lengths.

Appendix I.

Optical Circulator

I.1 Introduction

A practical way to modify a unidirectional fiber optic link either in communication or fiber optic laser amplifiers circuits is to use optical circulator. Optical circulator can be considered as a three or four port device.

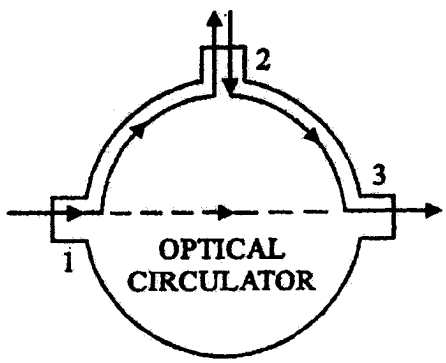

Fig.I.1 Optical circulator

In an optical circulator there are three main loss factors which can be denoted as "Insertion loss" , "Coupling loss" and "Cross talk (dashed line in Fig.I.1)". Basically, in circulator we need 90 degrees rotation for polarizations along the fiber axis which depends on the direction of beam. The procedure in a polarization independent circular is to divide an input beam into two linearly polarized beams whose vibration plates are perpendicular to each other. Beams first pass through a reciprocal rotator, which can be a polarization controller or half-wave plate or even twisted PMF and then pass through a non-reciprocal rotator, and finally they combine together.

I.2 Faraday Rotation

Faraday rotation is based on the asymmetry of the molecular structure. Even if two molecules contain the same atoms and bonds they may differ in their orientation relation to the coordinate system. Considering the circular birefringence in a crystal in which the right and left circularly polarized light meet different refractive index and taking into account that linearly polarized light is result of two circular polarization at the same amplitude but opposite in rotation, linear polarized light passing through the medium will show the rotation of its polarization direction. In another word, the degree of rotation is proportional to the difference between the refractive indices which is maximized by applying a magnetic field "H" along the magneto-optic medium and also proportional to the length of the path traversed, "L". So ,

$$Faraday\ Rotation \equiv \phi = HLV$$

where V is the verdet's constant which depends on the material and beam wavelength. So if we apply a uniform magnetic field over fiber we can transfer power from P_x , power of polarized light along X axis, to P_y. In another word, we can rotate the X polarized light toward Y axis for some degrees[1]. The clockwise or counter clockwise direction of rotation due to the Faraday effect depends on whether the direction of the external magnetic field applied to fiber is the same or opposite to the direction of light travel through fiber.

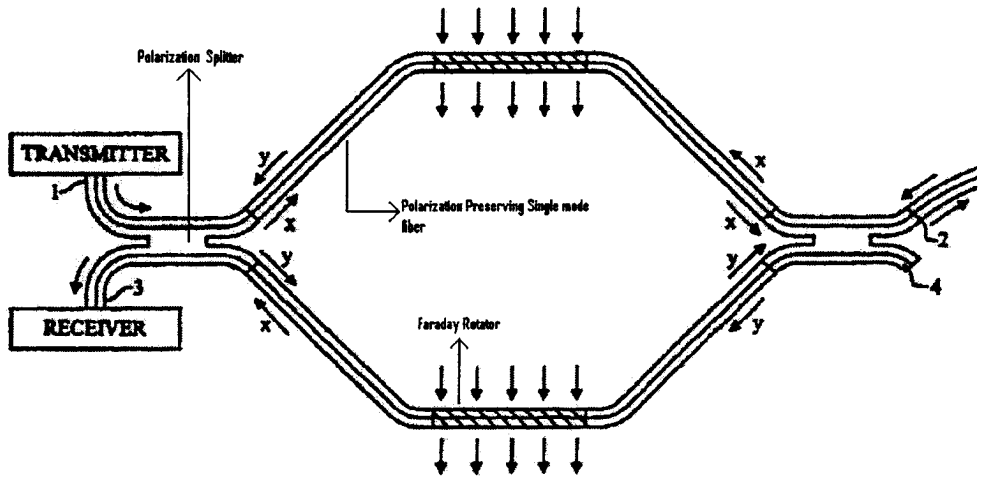

Fig.I.2 Polarization Independent All-Fiber Circulator

I.3 Description of all-fiber optical circulator function

Fig.I.2 shows the overall view of one three-port optical circulator function [2]. This optical circulator comprises a pair of all fiber polarization splitters, two Faraday rotators under the influence of a magnet which is strong enough to provide 45° nonreciprocal polarization rotation, and lengths of polarization preserving single mode fiber. Two opposite ends of polarization preserving fibers are spliced to Faraday rotator and the other two ends are spliced to polarization splitters. Faraday rotator comprises a polarization preserving single mode fiber which has been doped with one rare earth element like Terbium to increase the verdet constant. In order to have the reciprocal rotator in circulator, the polarization preserving single mode fibers are axially twisted totally to 45° measured from one end of fiber spliced to splitter to other end of fiber which is spliced to other polarization splitters. In another word, each fiber piece can be twisted individually 22.5° clockwise. When a randomly polarized light is emitted

through port "1" , polarization splitter divides it to two orthogonal linearly polarized light say, X *and* Y ,assuming that always Y polarized light is cross-coupled from one fiber in to another fiber within the splitter but X polarized light remains in the same fiber. Two 22.5° clockwise twists from each polarization preserving single mode fiber rotates each X *and* Y polarization states 45° clockwise but after passing through Faraday rotator the polarized light experiences 45° counter-clockwise rotation which totally makes the whole rotation experienced by each orthogonal polarizations become zero. After passing through second splitter Y polarized light again gets cross-coupled and combine with X polarized light which exits at the port "2". Considering the light emitted from port "2" which traverses from right to left , each splitted X *and* Y polarizations pass through non-reciprocal Faraday rotator and experience 45° rotation clockwise as well as additional 45° rotation clockwised by passing through twisted fiber lengths which eventually change the X polarized light to Y and Y to X. Again considering the cross-coupling for Y polarized light and maintaining the X polarized light at same fiber we will get the output at port "3".

REFRENCES:

1- R.H.Stolen,E.H.Turner "Faraday rotation in highly birefringence optical fiber" Appl. Opt., vol.19, no.6,pp.842-45,1980.

2- G.W.Pearson,J.S.Krasinski "Polarization independent all-fiber optical circulator," US. Pattent No.5400418,1995.

Appendix II.

Wavelength Division Multiplexing

II.1 Introduction

In order to increase transmission capacity and simultaneously transmit different signals together we should take advantage of wavelength division multiplexing / demultiplexing systems. Fig.II.1 shows two different configurations.

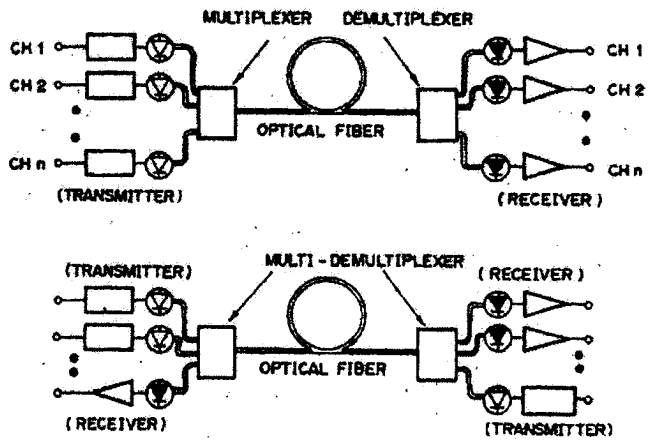

Fig. II.1 Fundamental configuration for WDM transmission

Optical Mux/Demux is mostly based on refractive device rather than tarnsmissive. Among all techniques which are used to make wavelength division multiplexing I here mention two techniques classified as angularly dispersive method and using Fiber Bragg Grating.

II.2.1 Angularly Dispersive Device

Angularly dispersive device is made of diffraction grating which reflects light in particular direction according to the grating constant, the incident angle of light and the optical wavelength. The angular properties of a grating are described by the grating equation (II.1)

$$Sin\, i + Sin\, \theta = \frac{m\lambda}{n\Lambda} \qquad \text{(II.1)}$$

where Λ is the grating period , m is the interference order and i and θ are the angles of incident and diffracted beams. If we rotate the grating and put that at the blaze angle of θ_B, called as Littrow mounted grating, in which $\theta \approx i$ we can minimize the

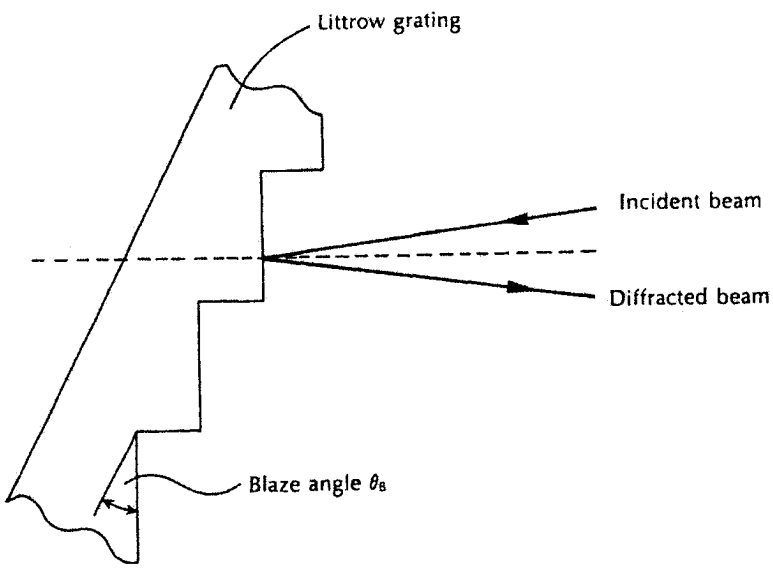

Fig.II.2 Littrow mounted diffraction grating

distortion .For a given center wavelength λ, we can find the blaze angle such that [1];

$$\theta_B = Sin^{-1}\left(\frac{\lambda}{2\Lambda}\right) \tag{II.2}$$

Considering $\theta \approx i$ and using equation (II.1) we can find the angular dispersion which is [2];

$$\frac{d\theta}{d\lambda} = \frac{2\tan\theta}{\lambda} \tag{II.3}$$

So, basically with using a blazed plane reflection grating and conventional lenses we can make a very simple and compact Mux/Demux .

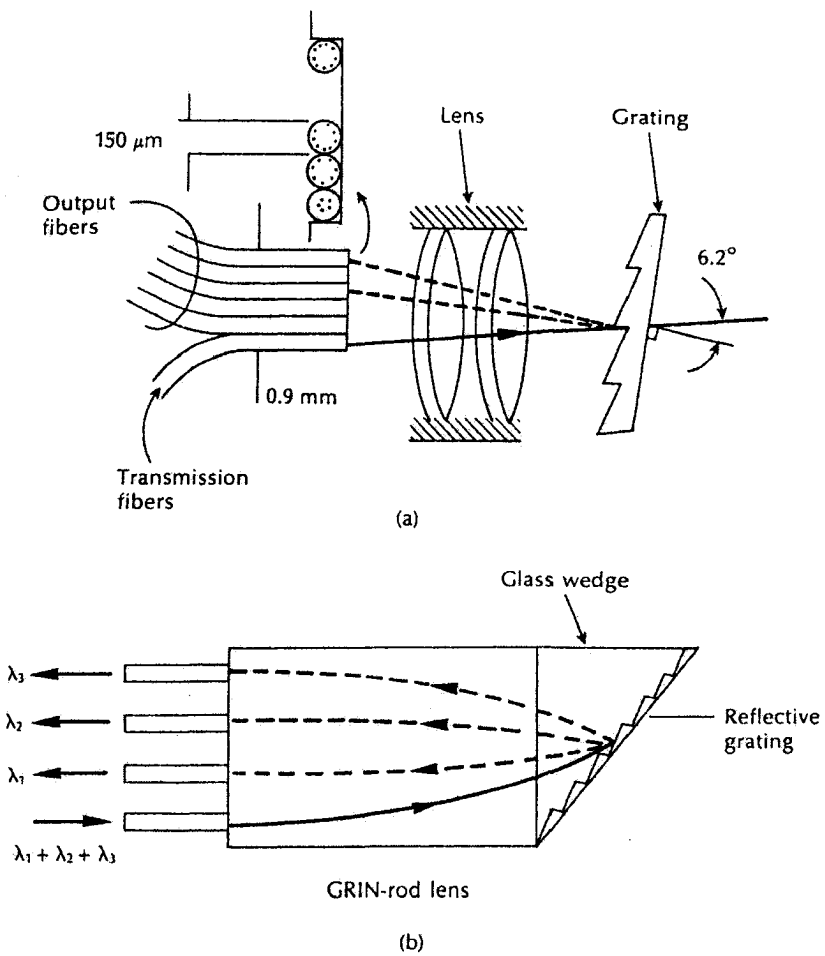

Fig .II. 3 Littrow type grating demux, (a) Using conventional lens (b) Using a GRIN rod lens

II.2.2 Fiber Bragg Grating (FBG)

With discovery of photosensitivity in optical fibers a new class of compact device which is called FBG has been introduced. FBG can basically function both as reflector and filter. FBG's consist of a periodic modulation of refractive index along the fiber core written by a standing wave pattern of an external light beam. In order to satisfy the bragg condition to have reflection from FBG near infra red $(\approx 1.55\,\mu m)$ the periodicity should written using UV wavelength. Another way to make Mux/Demux is using circulators in conjunction with Bragg grating allowing specific wavelength to be reflected and sent down like figure II.4,

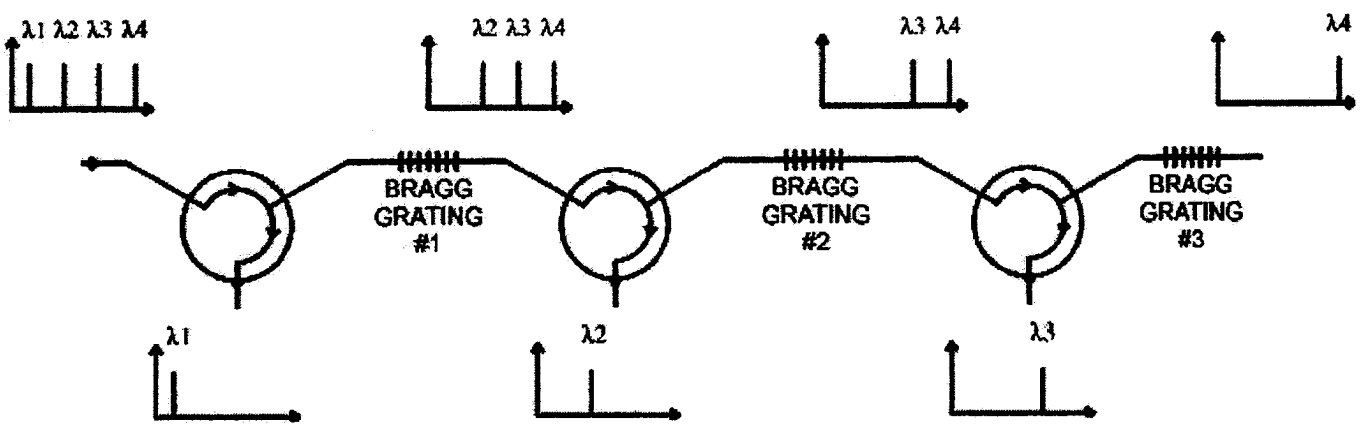

Fig.II.4 WDM Demux system using circulators

REFRENCES:

1- J.M.Senior; "Optical Fiber Communications, Principles and practice," Prentice Hall,1992.

2- H.Ishio,J.Minowa,K.Nosu "Review and status of wavelength-division –multiplexing technology and its application," J.Lightwave Techol.,vol.LT-2,no.4,pp.448-463,198

Appendix III

Multimode Power combiner

Power combiners provide an all-fiber high efficiency means of combining light from several multimode or single mode sources into one fiber to create high power output source. Output source can be used to pump optical amplifiers and fiber lasers. They are available in standard 3×1 , 6×1 configuration. They can be made by twisting and tapering a bundle of input fibers. Input fibers of bundle are matched to the pigtail fibers of diode sources. The resulting tapered fiber bundle is cleaved at the mid point and spliced to the output fiber. The data of power combiner we used is mentioned in Table III.1. In the experiments we used only one input port of coupler. What is most

SIFAM-TFB-550612B70	
Input fiber Core/Cladding (MM)	$\approx 105/125\ \mu m$
Input fiber NA	≈ 0.22
Output fiber Core/ Primary Cladding	$\approx 8/125\ \mu m$
Output fiber NA	≈ 0.45

Table III.1 Power combiner data

important to notice regarding the power combiners is that they should have high power transfer efficiency and they should be wavelength insensitive.